# Phosphoinositide kinase signaling controls ER-PM cross-talk

Deike J. Omnus[a,†], Andrew G. Manford[b,†], Jakob M. Bader[a], Scott D. Emr[b,*], and Christopher J. Stefan[a,b,*]
[a]MRC Laboratory for Molecular Cell Biology, University College London, London WC1E 6BT, United Kingdom; [b]Weill Institute for Cell and Molecular Biology, Department of Molecular Biology and Genetics, Cornell University, Ithaca, NY 14853

**ABSTRACT** Membrane lipid dynamics must be precisely regulated for normal cellular function, and disruptions in lipid homeostasis are linked to the progression of several diseases. However, little is known about the sensory mechanisms for detecting membrane composition and how lipid metabolism is regulated in response to membrane stress. We find that phosphoinositide (PI) kinase signaling controls a conserved PDK-TORC2-Akt signaling cascade as part of a homeostasis network that allows the endoplasmic reticulum (ER) to modulate essential responses, including $Ca^{2+}$-regulated lipid biogenesis, upon plasma membrane (PM) stress. Furthermore, loss of ER-PM junctions impairs this protective response, leading to PM integrity defects upon heat stress. Thus PI kinase–mediated ER-PM cross-talk comprises a regulatory system that ensures cellular integrity under membrane stress conditions.

## INTRODUCTION

The plasma membrane (PM) is highly organized and undergoes extensive remodeling via the delivery and removal of proteins and lipids. During membrane stress, PM quality control and recalibration systems ensure the integrity of the PM through the clearance of damaged PM components and by the delivery of newly synthesized materials (Zhao *et al.*, 2013). The biogenesis of proteins and lipids destined for the PM takes place in the endoplasmic reticulum (ER), which has essential roles in protein quality control, lipid biosynthesis, and calcium ($Ca^{2+}$) signaling (Friedman and Voeltz, 2011). ER metabolism must be modulated to adjust PM composition as needed. However, we do not fully understand how changes in PM composition and status are communicated to the ER.

The ER forms a continuous membrane network throughout the cell, consisting of nuclear ER, cytoplasmic sheets and tubules, and an extensive cortical meshwork (Friedman and Voeltz, 2011; Figure 1A depicts ER architecture in yeast). The ER engages in cross-talk with the PM through cortical ER-PM junctions, where the ER and PM form close connections without undergoing membrane fusion (Stefan *et al.*, 2013). ER-PM junctions are extensively formed in yeast by three conserved tether protein families: the VAP orthologues Scs2/Scs22, the extended synaptotagmin-like (E-Syt) proteins Tcb1/2/3, and the TMEM16 family member Ist2 (Manford *et al.*, 2012; Figure 1B). Loss of these ER-PM tethers results in a dramatic reduction of the cortical ER network and ER stress, indicating that ER-PM junctions control ER structure and function (Manford *et al.*, 2012; Δtether cells, Figure 1B). However, roles for ER-PM junctions in the regulation of PM organization and integrity have not been extensively characterized.

Here we show that ER-PM junctions are needed to maintain cellular integrity upon membrane stress. We find that phosphoinositide (PI) kinase signaling activates the yeast phosphoinositide-dependent kinase (PDK) orthologues Pkh1/Pkh2 and the target of rapamycin complex 2 (TORC2) upon stress conditions. Pkh1/2 and TORC2 activate the Akt/SGK protein kinase orthologues Ypk1/2 necessary for stress-induced sphingolipid synthesis in the ER (Roelants *et al.*, 2011; Berchtold *et al.*, 2012; Niles *et al.*, 2012; Sun *et al.*, 2012). Our results show that in cells lacking ER-PM tether proteins, Ypk1/2-stimulated sphingolipid synthesis in the ER is compromised, resulting in PM integrity defects. This is due to misregulation of $Ca^{2+}$ dynamics and
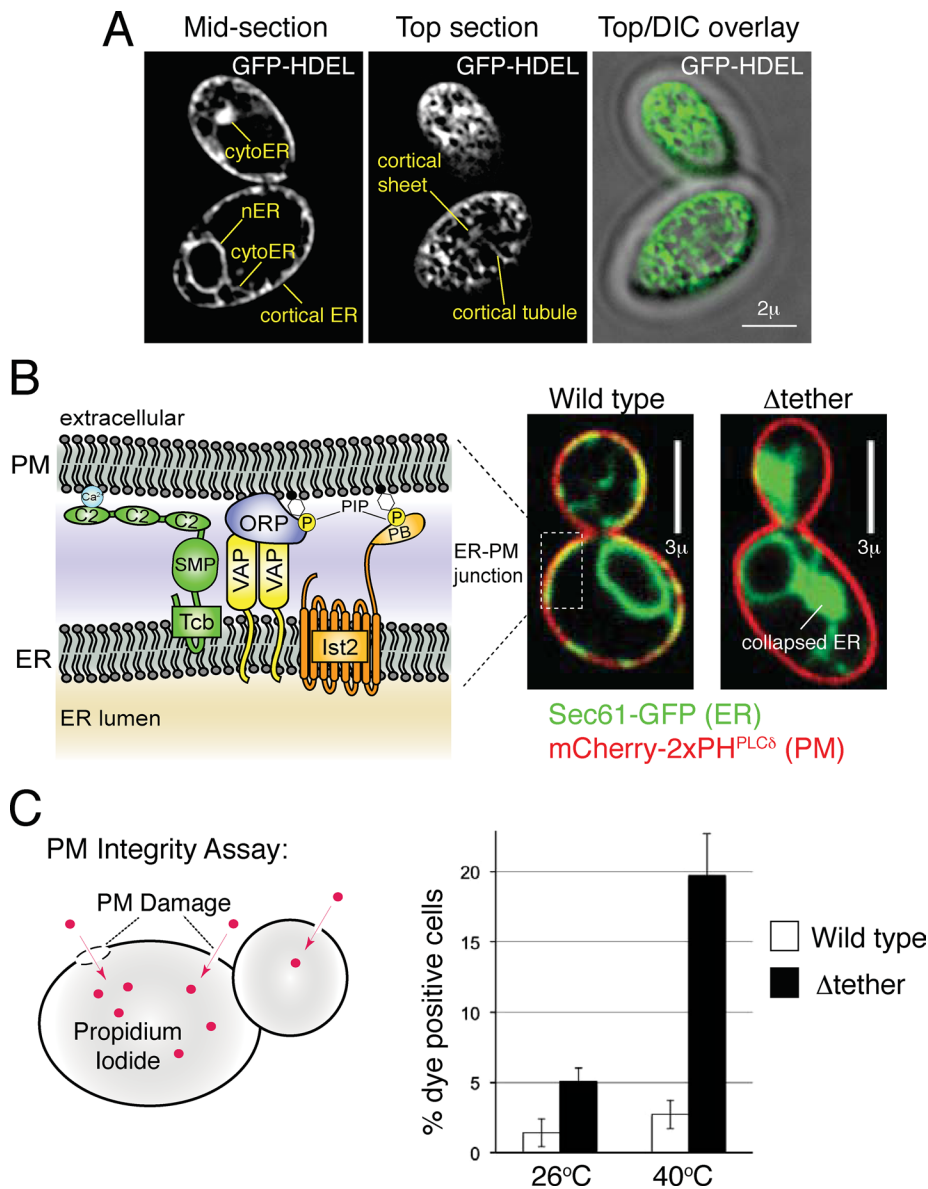
**FIGURE 1:** ER-PM junctions maintain PM integrity upon heat stress. (A) The ER forms an extensive network of sheets and tubules. Localization of the ER marker GFP-HDEL in wild-type diploid cells. Cortical ER (cER), cytoplasmic ER (cytoER), and nuclear ER (nER) are labeled. Scale bar, 2 µm. (B) Left, three protein families tether the cortical ER to the PM: the VAP proteins Scs2/22, Ist2, and the tricalbins (Tcb1/2/3). The VAP proteins bind PI4P-binding ORP family members. PB, polybasic domain; SMP, synaptotagmin-like mitochondrial lipid–binding protein. Right, loss of ER-PM tethers alters ER morphology. Localization of the ER marker Sec61-GFP (green) and PM marker mCherry-2xPH$^{PLC\delta}$ (red) in wild-type and Δtether cells (*ist2Δ, scs2/22Δ, tcb1/2/3Δ*). An ER-PM junction is indicated in wild-type cells and collapsed ER in Δtether cells. Scale bars, 3 µm. (C) Cells incubated at 26 or 40°C for 2 h were stained with propidium iodide to monitor PM integrity. Staining of wild-type (white bars) and Δtether (black bars) cells was analyzed by flow cytometry. See Supplemental Figure S1.

to changes in PM composition. Consistent with this, the cortical ER network is continuously remodeled in yeast cells and forms numerous contacts with the PM (Supplemental Movie S1). When followed over time (30 min), the cortical ER cumulatively covers >80% of the PM (Supplemental Movie S2). Accordingly, ER-PM contacts may allow the ER to sense the state of the PM (damage, composition) and launch responses (Ca$^{2+}$ dynamics, protein and lipid synthesis) to ensure PM integrity on changes in PM organization and stress conditions.

We examined whether ER-PM junctions are necessary to maintain PM integrity under stress conditions. These experiments used a quantitative flow cytometry assay measuring entry of the dye propidium iodide into yeast cells under various conditions (Figure 1 and Supplemental Figure S1; Zhao *et al.*, 2013). Propium iodide is membrane impermeant and can be used to score cells in a population that have lost cellular integrity. Wild-type yeast cells grown at 26°C exhibited negligible staining (<3% cells within the population; Figure 1C, 26°C). At 26°C, 5% of mutant cells lacking the ER-PM tether proteins (Δtether cells) stained with the dye, comparable to wild-type cells (Figure 1C). Wild-type cells were resistant to mild heat stress conditions (2 h at 40°C), with the PM remaining intact in the vast majority of the population (<4% of wild-type cells stain positive at 40°C; Figure 1C). However, Δtether cells showed increased sensitivity to heat stress. On incubation at 40°C, nearly 20% of the Δtether cells scored positive (fivefold greater than wild-type cells; Figure 1C). The Δtether cells also displayed dramatic sensitivity to brief heat shock at 42°C. Nearly 70% of the mutant cells scored as positive, compared with 5% of wild-type cells under these conditions (Supplemental Figure S1A). Among the individual tether family members, the Tcb1/2/3 proteins were particularly important. Approximately 45% of cells lacking Tcb1/2/3 displayed PM integrity defects upon brief heat shock at 42°C (compared with 15 and 5% of cells lacking the Scs2/22 VAP orthologues and Ist2 respectively; Supplemental Figure S1A). Cells lacking Tcb1/2/3 do not display an obvious reduc-

calcineurin signaling, which inhibits sphingolipid synthesis in the ER. Thus ER architecture and PI kinase–mediated ER-PM cross-talk play a central role in membrane homeostasis and cellular integrity.

## RESULTS

### ER-PM junctions maintain PM integrity during heat stress

The ER is a major site for protein biogenesis, lipid synthesis, and Ca$^{2+}$ homeostasis. Cross-talk between the ER and PM at membrane contact sites may regulate these important ER functions in response

tion in cortical ER (Manford *et al.*, 2012), suggesting that the tricalbins may be specifically needed for PM integrity rather than another ER-localized protein. Consistent with this, an artificial ER-PM tether protein (tandem PM-binding PH$^{PLC}\delta$ domains linked to the Scs2 ER-anchored transmembrane domain) formed cortical ER in the Δtether cells but did not restore PM integrity upon heat shock (Supplemental Figure S1, B and C). Thus proteins that form and function at ER-PM junctions (Tcb1/2/3 and Scs2/22) are specifically needed to maintain cellular integrity upon heat-induced PM damage.
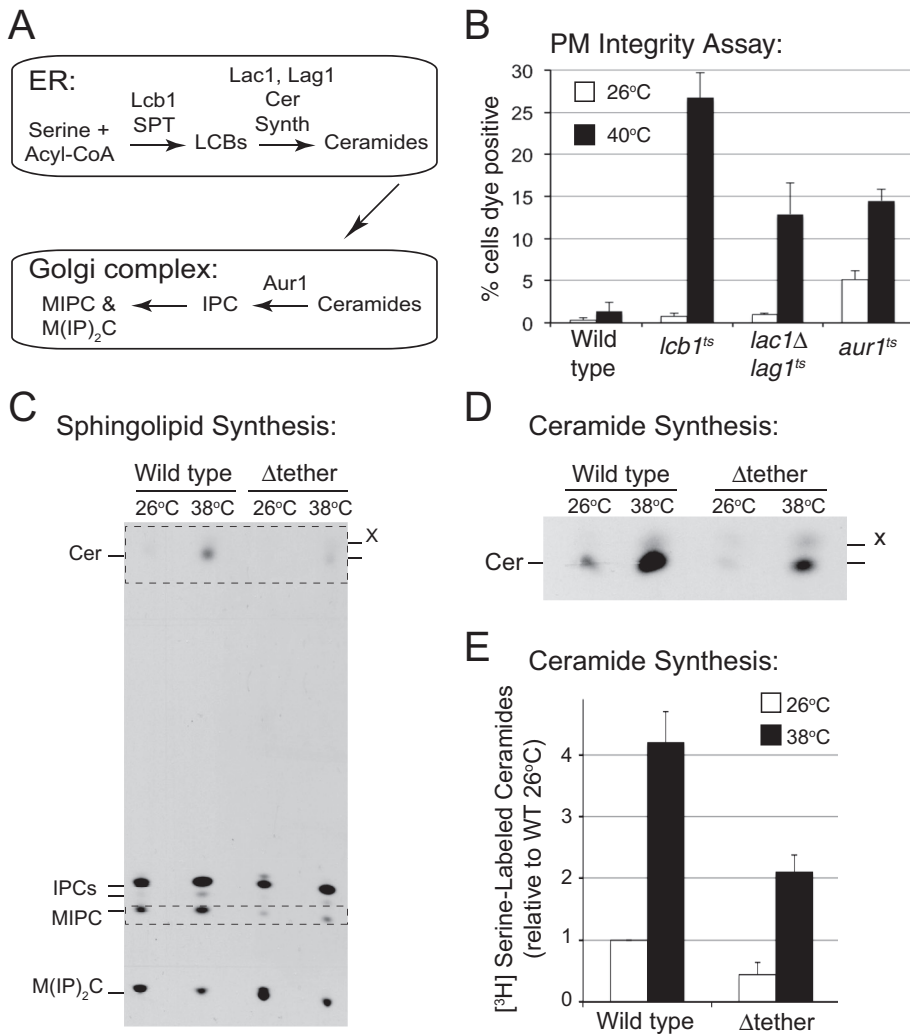
**A**

ER:

Serine + Acyl-CoA →[Lcb1 SPT] LCBs →[Lac1, Lag1 Cer Synth] Ceramides

Golgi complex:

MIPC & M(IP)$_2$C ← IPC ←[Aur1] Ceramides

**B**

PM Integrity Assay:

□ 26°C
■ 40°C

y-axis: % cells dye positive (0–30)

x-axis: Wild type, *lcb1*$^{ts}$, *lac1Δ lag1*$^{ts}$, *aur1*$^{ts}$

**C** Sphingolipid Synthesis:

Wild type (26°C, 38°C), Δtether (26°C, 38°C)

Cer — ... — X

IPCs
MIPC
M(IP)$_2$C

**D** Ceramide Synthesis:

Wild type (26°C, 38°C), Δtether (26°C, 38°C)

Cer — ... — x

**E** Ceramide Synthesis:

□ 26°C
■ 38°C

y-axis: [$^3$H] Serine-Labeled Ceramides (relative to WT 26°C) (0–4)

x-axis: Wild type, Δtether

**FIGURE 2:** ER-PM junctions regulate sphingolipid synthesis. (A) The yeast biosynthetic pathway for sphingolipid synthesis in the ER and Golgi network. (B) Sphingolipid synthesis in the ER and Golgi complex protects PM integrity during heat stress. Wild-type, *lcb1*$^{ts}$, *lac1 lag1*$^{ts}$, and *aur1*$^{ts}$ cells incubated at 26 (white bars) or 40°C for 2 h (black bars) were stained with propidium iodide and analyzed by flow cytometry. (C) Analysis of sphingolipid synthesis in wild-type and Δtether cells. Wild-type and Δtether cells were preincubated at the appropriate temperature for 10 min and labeled with [$^3$H]serine for 60 min. Sphingolipids were extracted and analyzed by TLC. Ceramides (Cer) and the complex sphingolipids IPCs, MIPC, and M(IP)$_2$C are indicated. An unknown lipid, X, was also observed. The hatched areas point out reduced ceramides and MIPC in the Δtether mutant cells. (D) Synthesis of ceramides in wild-type and Δtether cells. Results shown here are from a long exposure from an independent experiment to better visualize ceramides. As in Figure 2C, cells were preincubated at the appropriate temperature for 10 min and labeled with [$^3$H]serine for 60 min. Sphingolipids were extracted and analyzed by TLC. Ceramides (Cer) and an unknown lipid, X, are indicated. (E) Quantitation of ceramide synthesis in wild-type and Δtether cells normalized to wild type at 26°C. The data represent the mean ± SD from three independent experiments.

Elevated temperatures damage integral PM proteins, such as ion channels and nutrient transporters, activating a PM quality control pathway mediated by the ART protein E3 ubiquitin ligase adaptors (Zhao *et al.*, 2013). Misfolded PM proteins detected by the ARTs are marked with ubiquitin and targeted for endocytic internalization. After internalization, ubiquitinated damaged proteins are delivered to the endosomal sorting complexes required for transport (ESCRT)–mediated sorting pathway for degradation in vacuoles. Clearance of misfolded proteins from the cell surface is needed to maintain PM integrity, and loss of the ART proteins confers

reduced viability upon heat stress (Zhao *et al.*, 2013). However the ART- and ESCRT-mediated quality control pathways still function in cells lacking the ER-PM tether proteins. On heat stress (40°C), a green fluorescent protein (GFP)–tagged amino acid transporter, Can1-GFP, was internalized from the PM and delivered to the vacuole in both wild-type and Δtether cells (Supplemental Figure S1D). Thus the role for ER-PM contacts in PM integrity may be distinct from the quality control pathways carried out by the ART and ESCRT proteins.

**ER-PM junctions regulate sphingolipid synthesis necessary for PM integrity**

Cells up-regulate de novo sphingolipid synthesis in the ER during heat-induced membrane stress (Tabuchi *et al.*, 2006; Cowart and Hannun, 2007; Cowart and Obeid, 2007; Sun *et al.*, 2012; Muir *et al.*, 2014). We examined whether de novo sphingolipid synthesis is necessary to maintain PM integrity upon heat stress and whether ER-PM cross-talk is involved in this membrane stress response pathway. Sphingolipid synthesis is initiated in the ER, where long-chain sphingoid bases (LCBs) and ceramides are generated by the ER-localized serine palmitolyltransferase (SPT) and ceramide synthases, respectively (Figure 2A). We first examined whether de novo sphingolipid synthesis was necessary to maintain PM integrity upon heat stress. At 40°C, >25% of *lcb1*$^{ts}$ mutant cells (with impaired SPT activity) and 12% of *lac1 lag1*$^{ts}$ mutant cells (with impaired ceramide synthase activity) stained with propidium iodide (20- and 10-fold greater than wild-type cells, respectively; Figure 2B). In addition, 15% of *aur1*$^{ts}$ cells impaired in complex sphingolipid synthesis in the Golgi network displayed PM integrity defects upon shift to 40°C (Figure 2, A and B). Thus sphingolipid synthesis in the ER and Golgi compartments is needed for PM integrity during heat stress.

We next examined whether ER-PM junctions play a role in the regulation of sphingolipid synthesis. In [$^3$H]serine radiolabelling experiments, we observed that $^3$H-labeled ceramides increased greater than fourfold in wild-type cells upon heat stress conditions (Figure 2, C–E, 26 vs. 38°C), consistent with previous studies (Tabuchi *et al.*, 2006; Cowart and Hannun, 2007; Cowart and Obeid, 2007; Sun *et al.*, 2012; Muir *et al.*, 2014). However, [$^3$H]serine-labeled ceramides were significantly reduced in the Δtether cells (50% of wild-type levels at both 26 and 38°C; Figure 2, C–E). Ceramides are converted to more complex sphingolipids in the Golgi network (Figure 2A), including the yeast complex sphingolipids inositolphosphoceramides (IPCs) and mannosylinositolphosphoceramides (MIPC and M(IP)$_2$C). Incorporation of $^3$H-labeled serine into IPC and M(IP)$_2$C was not significantly

affected, but MIPC synthesis was reduced in the Δtether cells as compared with wild-type cells (48 and 70% of wild-type levels at 26 and 38°C, respectively; Supplemental Figure S2, A and B). The Δtether mutant cells were also hypersensitive to aureobasidin A, an inhibitor of Aur1 activity and sphingolipid synthesis in the Golgi complex (Supplemental Figure S2C), further suggesting that sphingolipid synthesis is impaired in these cells. Expression of the artificial ER-PM tether protein did not rescue the hypersensitivity of the Δtether mutant cells to aureobasidin A (Supplemental Figure S2C). Taken together, these results suggest that 1) ER-PM tether proteins are specifically involved in the control of sphingolipid synthesis and 2) sphingolipid synthesis defects in the Δtether mutant cells may result in PM integrity defects upon stress conditions.

## Pkh1 and TORC2 signaling link PI kinase signaling at the PM to sphingolipid synthesis in the ER

We next investigated how ER-PM cross-talk is regulated and the role for ER-PM junctions in membrane stress responses. PI kinases localized at the PM are required for cellular integrity and responses to heat stress (Audhya et al., 2000; Audhya and Emr, 2002). At elevated temperature, levels of phosphatidylinositol 4-phosphate (PI4P) and phosphatidylinositol (4,5)-bisphosphate (PI(4,5)P$_2$) generated by the Stt4 PI4K and the Mss4 PI4P 5-kinase are modestly increased (Audhya and Emr, 2002). Stt4 PI4K and Mss4 PI4P5K activities have also been implicated in sphingolipid metabolism (Tabuchi et al., 2006). However, roles for PI kinase signaling in the regulation of ER-PM cross-talk and membrane stress responses have not been fully elucidated.

The yeast protein kinases 1 and 2 (Ypk1/2), orthologues of mammalian Akt, regulate sphingolipid synthesis in the ER. Ypk1/2 phosphorylate and inactivate the Orm1/2 proteins, integral ER membrane proteins that inhibit SPT, the first enzyme in sphingolipid biosynthesis (Roelants et al., 2011; Berchtold et al., 2012; Sun et al., 2012; Gururaj et al., 2013). Ypk1/2 also phosphorylate and activate ceramide synthases in the ER (Muir et al., 2014). Activation of Ypk1/2 occurs through two upstream protein kinases, the PDK orthologues Pkh1/Pkh2 and TORC2; Roelants et al., 2004; Niles et al., 2012). TORC2 signaling in yeast cells is regulated by the PI(4,5)P$_2$-binding Slm1 and Slm2 proteins (Audhya et al., 2004; see later discussion of Figure 5). However, it is unclear whether PI kinase signaling regulates the yeast PDK orthologues Pkh1 and Pkh2.

We addressed whether PI kinase and TORC2-Pkh1/2-Ypk1/2 signaling function together in ER-PM cross-talk. Loss of Stt4, Mss4, Pkh1/2, or Ypk1/2 function similarly resulted in severe PM integrity defects even upon brief heat shock conditions (42°C, 10 min). At 42°C, 60% of stt4$^{ts}$ mutant cells and 50% of mss4$^{ts}$, pkh1$^{ts}$ pkh2, and ypk1$^{ts}$ ypk2 mutant cells stained with propidium iodide (10-fold greater than wild-type cells; Figure 3A). Moreover, overexpression of Ypk1 partially rescued the growth defects of stt4$^{ts}$ mutant cells (Supplemental Figure S3A), suggesting that Ypk1 function may be impaired in cells with reduced Stt4 PI4K activity. Altogether, these results suggested that Stt4, Mss4, Pkh1/2, and Ypk1/2 function in a similar pathway, and we further investigated roles for PI kinases in Pkh1/2 and Ypk1/2 signaling.

The PDK orthologues Pkh1/2 phosphorylate the activation loops of Ypk1 and Ypk2 (residue T504 in Ypk1; Roelants et al., 2004). We tested whether Stt4 and Mss4 PI kinase activities control Pkh1/2 signaling, using an antibody that recognizes Ypk1 phosphorylated at residue T504. On heat stress (at 38°C), phospho-Ypk1(T504) increased more than threefold in wild-type cells (Figure 3B and Supplemental Figure S3B). As a control, phospho-Ypk1(T504) levels were barely detectable in pkh1$^{ts}$ pkh2 mutant cells (Figure 3B and
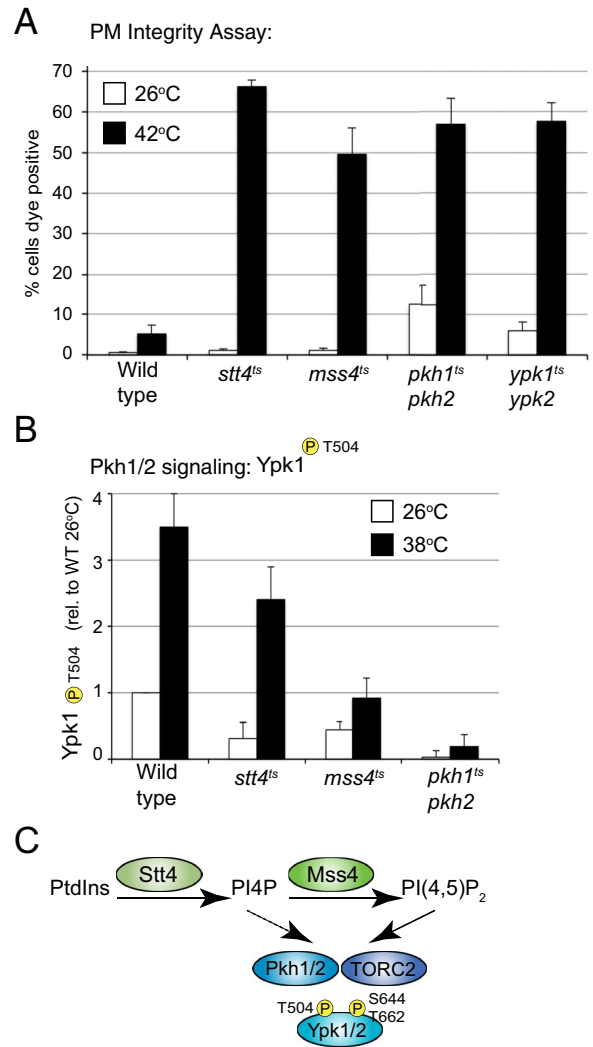


FIGURE 3: PI kinase signaling regulates the protein kinase Pkh1.
(A) Wild-type, stt4$^{ts}$, mss4$^{ts}$, pkh1$^{ts}$ pkh2Δ, and ypk1$^{ts}$ ypk2Δ cells incubated at 26 (white bars) or 42°C for 10 min (black bars) were stained with propidium iodide and analyzed by flow cytometry to monitor PM integrity. (B) Pkh1/2 signaling is modestly impaired in stt4$^{ts}$ and strongly impaired in mss4- cells. Wild-type, stt4$^{ts}$, mss4$^{ts}$, and pkh1$^{ts}$ pkh2Δ cells were incubated at 26 or 38°C for 2 h. Protein extracts were analyzed by immunoblotting using antisera that recognize phospho-Ypk1(T504). Levels of phospho-Ypk1(T504), normalized to a protein loading control, are shown relative to wild-type cells at 26°C. Results are the mean ± SD from three independent experiments. See Supplemental Figure S3B. (C) Speculative model for regulation of Ypk1/2 signaling by Pkh1/2, TORC2, and the PI isoforms PI4P and PI(4,5)P$_2$. PI(4,5)P$_2$ is essential for Pkh1/2 signaling, but PI4P may be involved in Pkh1/2 regulation as well (dashed arrow).

Supplemental Figure S3B). Phospho-Ypk1(T504) was modestly reduced in stt4$^{ts}$ cells (30 and 68% of control levels at 26 and 38°C, respectively; Figure 3B and Supplemental Figure S3B). In mss4$^{ts}$ mutant cells, phospho-Ypk1(T504) levels were significantly reduced (44 and 26% of control levels at 26 and 38°C, respectively; Figure 3B and Supplemental Figure S3B). As a control, Ypk1 expression levels were slightly elevated in pkh1$^{ts}$ pkh2, stt4$^{ts}$, and mss4$^{ts}$ mutant cells (2-, 1.3-, and 1.6-fold, respectively, at 38°C; Supplemental Figure S3C), indicating that reduced phospho-Ypk1(T504) levels in the

mutant cells were not simply due to lower Ypk1 expression. Taking Ypk1 levels into account, phospho-Ypk1(T504):Ypk1 ratiometric levels in $stt4^{ts}$ and $mss4^{ts}$ mutant cells were 52 and 16% of wild-type levels, respectively, at the restrictive temperature. These results suggested that both Stt4 and Mss4 were needed for full Pkh1/2 signaling, although the Mss4 PI4P 5-kinase and its product, PI(4,5)P$_2$, are critical regulators of Pkh1/2 signaling.

Next we examined Pkh1 subcellular localization under normal and heat shock conditions using a functional GFP-Pkh1 fusion expressed from its own promoter (Figure 4 and Supplemental Figure S4, A and B). In wild-type cells at 26°C, GFP-Pkh1 was mainly diffuse throughout the cytoplasm (Figure 4, A and C, and Supplemental Figure S4, C and F), but small, cortical puncta (one to three per cell) could be observed in cells (Figure 4, A and C arrows). On heat shock at 42°C, there was a measurable increase in the number of cortical GFP-Pkh1 foci per cell (Figure 4, A and B, and Supplemental Figure S4, C and F), as well as of puncta size and intensity. The enlarged GFP-Pkh1 foci at 42°C appeared to be mainly cortical, although intracellular puncta were also observed (Figure 4 and Supplemental Figure S4).

A previous study demonstrated that the Pkh1 protein binds liposomes containing various PI lipids or LCBs in vitro (Gallego et al., 2010). We examined roles for the PI isoforms PI4P and PI(4,5)P$_2$ as well as LCBs in Pkh1 localization in vivo. Pretreatment with the PI4K inhibitor phenylarsine oxide (PAO) impaired heat shock–induced formation of GFP-Pkh1 puncta (Supplemental Table S3), suggesting a role for PI lipids. However, upon brief heat shock conditions (10 min at 42°C; Supplemental Table S3), neither Stt4 nor Mss4 activity appeared to be specifically required, suggesting that both PI4P and PI(4,5)P$_2$ may target Pkh1 to the PM. Accordingly, GFP-Pkh1 puncta were increased in $sjl1$ $sjl2^{ts}$ $sjl3$ mutant cells impaired in synaptojanin activity required for efficient PI(4,5)P$_2$ turnover (Supplemental Table S3). PI4P availability is increased at the PM upon heat-induced membrane stress (Supplemental Figure S4C; Jesch et al., 2010), and in support of a role for PI4P in GFP-Pkh1 localization, the size and number of GFP-Pkh1 foci at 26°C increased in $sac1\Delta$ cells and $\Delta$tether cells, which have elevated PI4P levels but not PI(4,5)P$_2$ (Figure 4, C and D, and Supplemental Table S3; Manford et al., 2012). As a control, expression of GFP-Pkh1 was not increased in $sac1$ cells and $\Delta$tether cells as compared with wild type (Supplemental Figure S4B).

LCBs have also been suggested to regulate Pkh1/2 function in vivo (Liu et al., 2005), and LCBs are elevated in cells lacking the Sac1 PI4P phosphatase activity (see later discussion of Figure 6A; Brice et al., 2009; Breslow et al., 2010). However, GFP-Pkh1 remained localized to punctate structures in $sac1$ mutant cells treated with myriocin, which blocks LCB synthesis (Supplemental Figure S4D; 3–10 puncta/cell), indicating that increased PI4P levels may be sufficient for Pkh1 membrane recruitment. Consistent with this, the intensity of GFP-Pkh1 assemblies decreased in $stt4^{ts}$ $sac1\Delta$ double mutant cells as compared with $sac1\Delta$ single-mutant cells (Supplemental Figure S4E). Moreover, GFP-Pkh1 puncta were not significantly increased at 26 or 42°C in $orm1$ $orm2$ mutant cells, which have elevated LCB levels (Supplemental Figure S4F and Supplemental Table S3; see later discussion of Figure 6A; Brice et al., 2009; Breslow et al., 2010).

Taken together, these results suggest that both PI4P and PI(4,5)P$_2$ may be involved in targeting Pkh1 to the PM, although PI(4,5)P$_2$ is a primary regulator of phosphorylation of Ypk1 by Pkh1 (Figure 3; see later discussion). In addition, the data indicate that Pkh1 signaling is not disrupted in the $\Delta$tether mutant cells. The Scs2/22, Tcb1/2/3, and Ist2 proteins apparently are not required for formation of cortical Pkh1 assemblies, as Pkh1 was constitutively recruited to the PM in
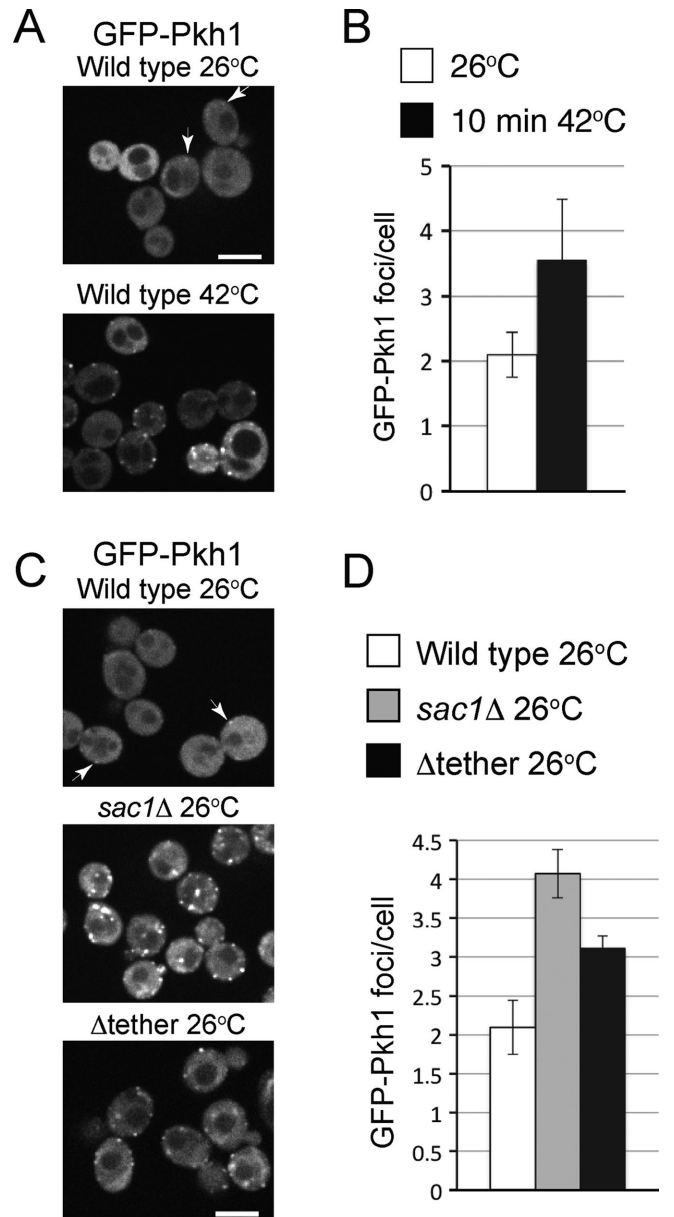


**FIGURE 4:** Heat-induced membrane stress and PI metabolism regulate Pkh1 localization. (A) Pkh1 assembles into cortical patches upon heat shock. Wild-type cells expressing GFP-Pkh1 were grown at 26°C (top) and shifted to 42°C for 10 min (bottom). Arrows show examples of small GFP-Pkh1 cortical patches in wild-type cells at 26°C. The majority of GFP-Pkh1 foci are cortical, but internal patches are also observed. Scale bar, 5 μm. See Supplemental Figure S4C. (B) High-content quantitative analysis of GFP-Pkh1 distribution. Maxima for GFP-Pkh1 foci in single focal planes (1482 foci in total from 720 cells at 26 and 3742 foci in total from 1095 cells after heat shock at 42°C) were identified using Fiji. Results show the mean and SD from three independent experiments. (C) PI4P metabolism controls Pkh1 localization. GFP-Pkh1 localization in wild-type, $sac1\Delta$, and $\Delta$tether cells. Arrows show examples of small GFP-Pkh1 cortical patches in wild-type cells at 26°C. GFP-Pkh1 puncta are increased in $sac1\Delta$ and $\Delta$tether cells at 26°C. Scale bar, 5 μm. (D) GFP-Pkh1 puncta are increased in $sac1\Delta$ and $\Delta$tether cells. Maxima for GFP-Pkh1 foci in single focal planes (1482 in total from 720 wild-type cells, 7258 in total from 1802 $sac1\Delta$ cells, and 3921 in total from 1261 $\Delta$tether cells at 26°C) were identified using Fiji. Results show the mean and SD from three independent experiments. See Supplemental Figure S4, D–F.
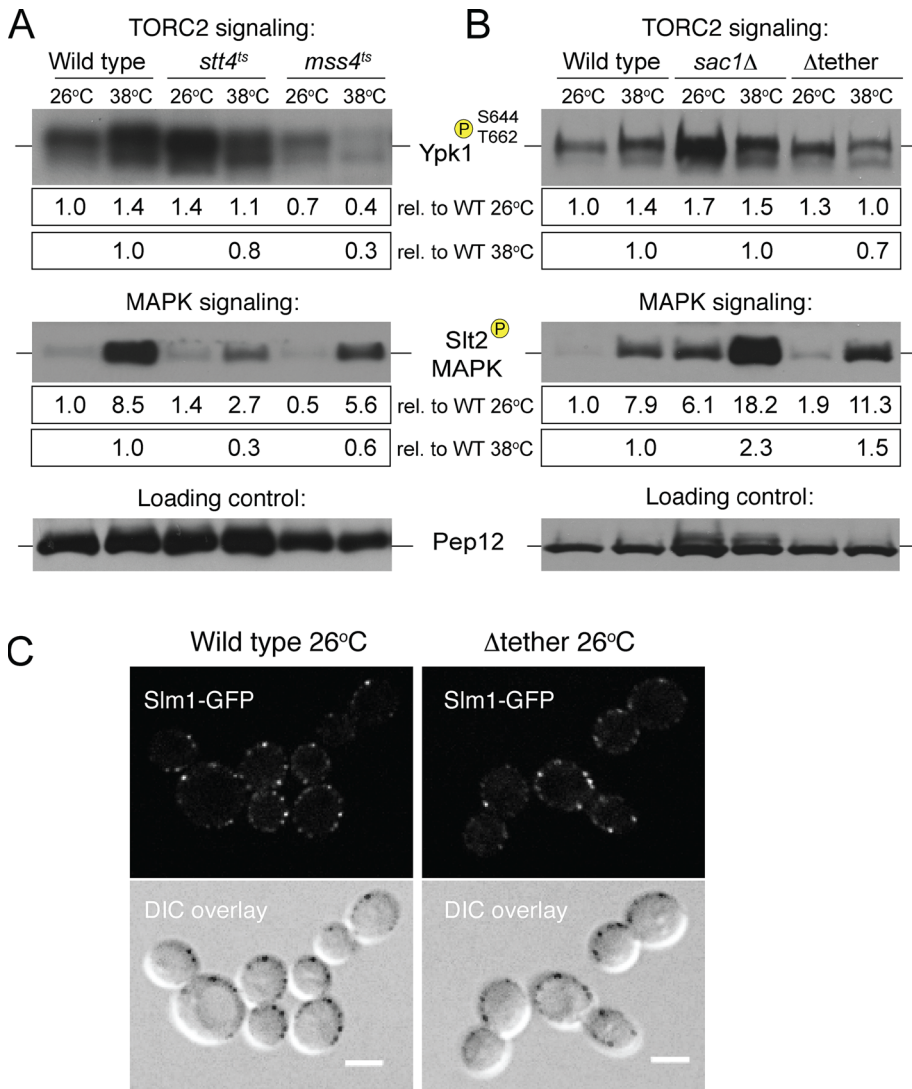
**A** TORC2 signaling:

| | Wild type | | stt4ts | | mss4ts | |
|---|---|---|---|---|---|---|
| | 26°C | 38°C | 26°C | 38°C | 26°C | 38°C |

Ypk1 (P) S644 T662

| 1.0 | 1.4 | 1.4 | 1.1 | 0.7 | 0.4 | rel. to WT 26°C |
|---|---|---|---|---|---|---|
| 1.0 | | 0.8 | | 0.3 | | rel. to WT 38°C |

MAPK signaling:

Slt2 (P) MAPK

| 1.0 | 8.5 | 1.4 | 2.7 | 0.5 | 5.6 | rel. to WT 26°C |
|---|---|---|---|---|---|---|
| 1.0 | | 0.3 | | 0.6 | | rel. to WT 38°C |

Loading control:

Pep12

**B** TORC2 signaling:

| | Wild type | | sac1Δ | | Δtether | |
|---|---|---|---|---|---|---|
| | 26°C | 38°C | 26°C | 38°C | 26°C | 38°C |

| 1.0 | 1.4 | 1.7 | 1.5 | 1.3 | 1.0 | |
|---|---|---|---|---|---|---|
| 1.0 | | 1.0 | | 0.7 | | |

MAPK signaling:

| 1.0 | 7.9 | 6.1 | 18.2 | 1.9 | 11.3 | |
|---|---|---|---|---|---|---|
| 1.0 | | 2.3 | | 1.5 | | |

Loading control:

**C** Wild type 26°C    Δtether 26°C

Slm1-GFP    Slm1-GFP

DIC overlay    DIC overlay

**FIGURE 5:** PI4P and PI(4,5)P$_2$ metabolism control TORC2 signaling. (A) TORC2 signaling and Slt2 MAPK phosphorylation in wild-type, stt4ts, and mss4ts cells. Wild-type (WT), stt4ts, and mss4ts cells were incubated at 26 or 38°C for 2 h. Protein extracts were analyzed by immunoblotting using antisera that recognize phospho-Ypk1(T662) or phospho-Slt2. Quantifications below the blot report the difference relative to WT after normalizing to a protein loading control; results are the mean of three independent experiments. (B) TORC2 signaling and Slt2 MAPK phosphorylation in cells lacking the PI4P phosphatase Sac1 or the ER-PM tether proteins. WT, sac1Δ, and Δtether cells were incubated at 26 or 38°C for 2 h. Protein extracts were analyzed by immunoblotting using antisera that recognize phospho-Ypk1(T662) or phospho-Slt2. Quantifications below the blot report the difference relative to WT after normalizing to a protein loading control; results are the mean of three independent experiments. See Supplemental Figure S5. (C) Slm1-GFP localization in WT cells (left) and Δtether cells (right). Bottom, differential interference contrast overlays. Scale bar, 5 μm.

TORC2 (Audhya et al., 2004; Niles et al., 2012). We further investigated roles for PI lipids and ER-PM junctions in TORC2 signaling during heat-induced membrane stress. Phosphorylation of Ypk1 by TORC2 increased upon heat stress, as measured by antisera that detect phospho-Ypk1(S644, T662; Figure 5). As expected, mss4ts mutant cells displayed significantly reduced TORC2 signaling (30% of wild-type levels at 38°C; Figure 5A). This could also result in significantly reduced phospho-Ypk1(T504) levels observed in mss4ts mutant cells (Figure 3), because the PI(4,5)P$_2$-binding Slm1/2 proteins and TORC2 promote phosphorylation of Ypk1 by Pkh1/2 (Roelants et al., 2004; Niles et al., 2012). Heat-induced Ypk1 phosphorylation by TORC2 was also impaired in stt4ts mutant cells (38°C, Figure 5A), possibly because Stt4-generated PI4P is used for PI(4,5)P$_2$ synthesis by Mss4 (Audhya et al., 2000; Audhya and Emr, 2002). As a control, the MAPK Slt2 was hypophosphorylated in stt4 and mss4 mutant cells at the restrictive temperature (Figure 5A), consistent with a previous study (Audhya and Emr, 2002).

Of interest, levels of phospho-Ypk1(S644, T662) were increased in stt4ts, sac1Δ, and the Δtether mutant cells at 26°C (Figure 5, A and B). Membrane stress caused by disruptions in sphingolipid metabolism results in activation of TORC2 signaling (Berchtold et al., 2012). Accordingly, the constitutive TORC2 signaling at 26°C observed in stt4ts, sac1, and Δtether mutant cells alike could be due to alterations in sphingolipid metabolism in these cells (Tabuchi et al., 2006; Brice et al., 2009; Breslow et al., 2010; Figures 3 and 6A). Consistent with this idea, pkh1ts pkh2 double-mutant cells also displayed increased TORC2 signaling, as phospho-Ypk1(S644, T662) levels were elevated 6.7- and 6.5-fold above wild-type levels at 26 and 38°C, respectively (Supplemental Figure S5). Alternatively, elevated phospho-Ypk1(S644, T662) levels in pkh1ts pkh2Δ, stt4ts, sac1Δ, and Δtether mutant cells at 26°C could simply be due to increased Ypk1 protein levels in these cells (Supplemental Figure S3; unpublished data).

On heat stress, phospho-Ypk1(S644, T662) levels were slightly reduced in the Δtether mutant cells (70% of wild-type levels at 38°C; Figure 5B). However, impaired TORC2 signaling cannot readily explain the sphingolipid synthesis defects observed in the Δtether cells. Sphingolipid synthesis was compromised in the Δtether cells even at 26°C (Figure 2), whereas TORC2 signaling was not impaired (and even increased) at this temperature (Figure 5B). Consistent with this idea, Slm1-GFP localized to cortical patches in both wild-type and Δtether mutant cells (Figure 5C). Thus ER-PM junctions are not necessarily required for Pkh1/2 and TORC2 localization and function. In the Δtether mutant cells, Pkh1 and TORC2 still localize to the PM and phosphorylate Ypk1, but

cells lacking these proteins. In line with this, phospho-Ypk1(T504) levels in the Δtether mutant cells resembled wild-type control levels (Supplemental Figure S3B). Thus the sphingolipid synthesis defects in the Δtether mutant cells cannot simply be explained by reduced Pkh1 signaling or defects in targeting Pkh1 to the PM.

Ypk1 activation also requires phosphorylation at residues S644 and T664 by TORC2. Phosphorylation of Ypk1 by TORC2 facilitates phosphorylation of Ypk1 by Pkh1, resulting in full Ypk1 activity (Roelants et al., 2011; Niles et al., 2012). TORC2 signaling is regulated by the PH domain–containing proteins Slm1 and Slm2, which bind PI(4,5)P$_2$ and recruit Ypk1 to the PM for phosphorylation by

**A** Sphingolipid synthesis:

wildtype  Δtether  sac1Δ  orm1,2Δ

X
Cer
LCB — ⟨LCB⟩
IPCs
MIPC
LCB(P) — ⟨LCB(P)⟩
M(IP)$_2$C
origin

**B** Ypk1/2 (Akt) sites:

Consensus..... RXRX**S** ....
Lag1..............$_{18}$TRRRN**SS**$_{24}$....
Lac1..........$_{18}$RPRRK**SS**$_{24}$....

Cer / Cer Syn / cyto / ER lumen / N / COOH

**C** Ceramide synthesis:

*lag1$^{ts}$ lac1* cells:

+Lag1        +Lag1$^{S23,24E}$
26°C  38°C   26°C  38°C

Cer

**D** phostag gel:

wild type  wild type  Δtether  ypk1$^{ts}$ ypk2
EV         + Lag1-GFP

Lag1(P)-GFP
Lag1-GFP

Loading control (SDS PAGE):

PGK

**E**

phospho-Lag1-GFP (% of total Lag1-GFP)

15
10
5
0

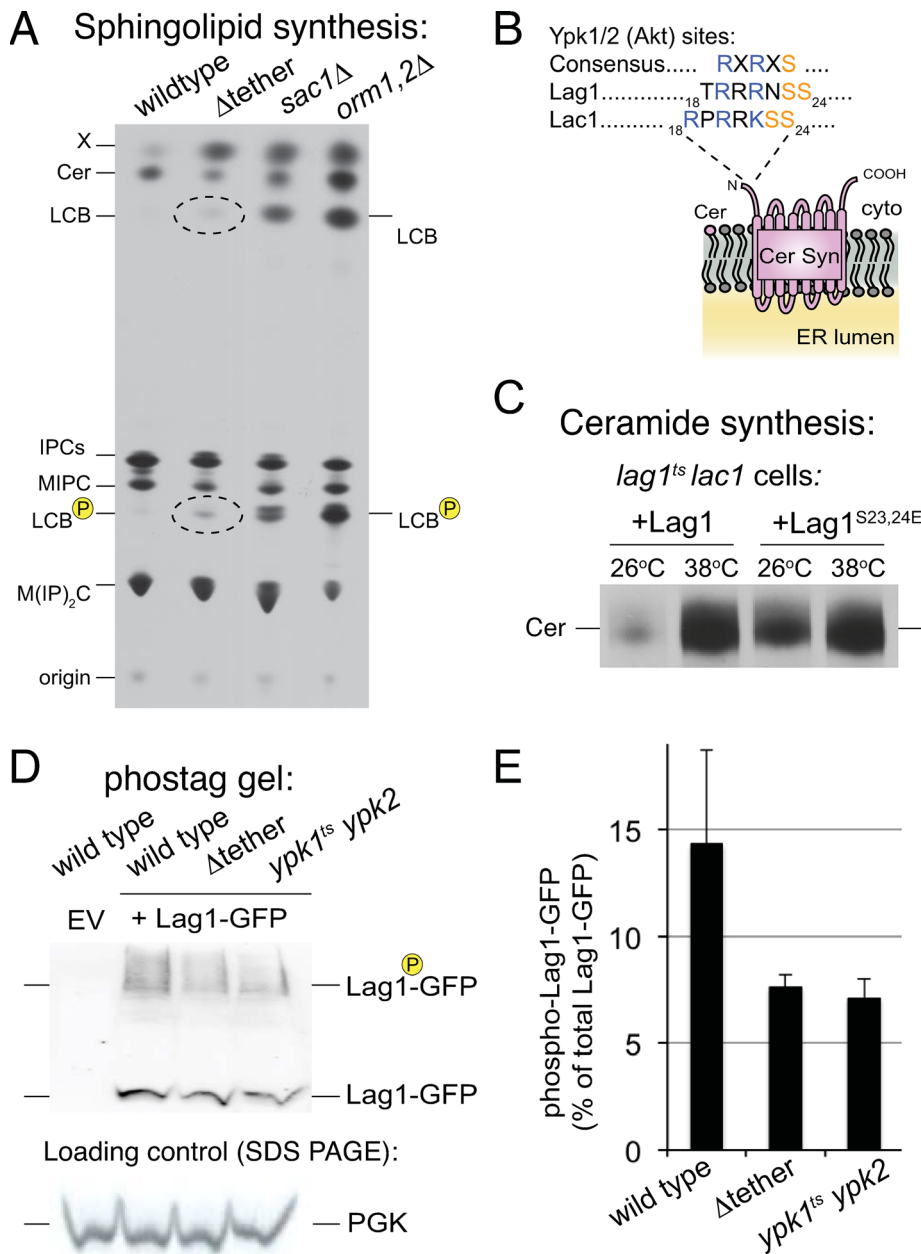wild type  Δtether  ypk1$^{ts}$ ypk2

**FIGURE 6:** ER-PM cross-talk controls ceramide synthase activity in the ER. (A) Synthesis of ceramides, but not LCBs, is compromised in the Δtether cells. Wild-type, Δtether, sac1Δ, and orm1Δ orm2Δ cells were labeled with [³H]serine for 60 min at 26°C. Sphingolipids were extracted and analyzed by TLC. LCBs, phosphorylated-LCBs (LCB-P), ceramides (Cer), and other sphingolipid species are indicated. The hatched ovals point out elevated LCBs and phosphorylated LCBs in the Δtether mutant cells. In addition, note that ceramides are reduced in the Δtether mutant cells as compared with wild-type cells (Figure 2). The sac1Δ and orm1Δ orm2Δ cells serve as controls for LCBs and phosphorylated LCBs. See Supplemental Figure S6, A and B. (B) Schematic cartoon depicting topology of Lac1 and Lag1 in the ER. Both proteins possess Ypk1/2 consensus sites in their N-terminal cytoplasmic tails. (C) Double-mutant lac1Δ lag1$^{ts}$ cells expressing either wild-type Lag1 or the phosphomimetic form Lag1$^{S23,24E}$ from plasmids were preincubated at the appropriate temperature for 10 min and labeled with [³H]serine for 60 min. Sphingolipids were extracted and analyzed by TLC. (D) Analysis of Lag1-GFP phosphorylation upon heat stress conditions. Wild-type, Δtether, and ypk1$^{ts}$ ypk2Δ cells expressing Lag1-GFP were incubated at 38°C for 2 h. Protein extracts were prepared, separated by Phos-tag gel electrophoresis, and analyzed by immunoblotting using an antibody that specifically recognizes GFP. Wild-type cells carrying empty vector were included as a control for the GFP antisera. SDS–PAGE and immunoblotting were used to determine expressions levels of PGK as a protein loading control. (E) Quantitation of phosphorylated Lag1-GFP level in wild-type and Δtether cells as a percentage of total Lag1-GFP protein levels. The data represent means ± SDs from two independent experiments analyzed in duplicate.

Ypk1 signaling may not be effectively transduced to targets involved in sphingolipid synthesis in the ER.

**ER-PM junctions modulate cytoplasmic Ca²⁺ and calcineurin to control Ypk1-regulated lipid synthesis in the ER**

We next investigated why sphingolipid synthesis in the ER was impaired in the Δtether cells (Figure 2). We found that synthesis of LCBs and phosphorylated LCBs was not compromised in the Δtether cells. Instead, levels of LCBs and phospho-LCBs were increased relative to wild-type cells at 26°C (Figure 6A), although not nearly to the extent as sac1 and orm1 orm2 mutant cells known to have increased LCB species (Figure 6A; Brice et al., 2009; Breslow et al., 2010). The Δtether cells were also resistant to myriocin, which inhibits LCB synthesis in the ER, and the myriocin-resistant phenotype was not rescued by expression of the artificial tether protein (Supplemental Figure S6, A and B). The accumulation of LCBs (Figure 6A) and decrease in ceramides (Figure 2) suggested that ceramide synthesis might be a rate-limited step in the Δtether cells.

Ypk1/2 phosphorylate and activate the ceramide synthases Lag1 and Lac1 at consensus sites within their N-terminal cytoplasmic tails (Figure 6B; Muir et al., 2014). Consistent with this, basal ceramide synthesis was increased (nearly 80% of heat-induced levels) in cells expressing a phosphomimetic form of Lag1 from a plasmid (S23E, S24E; Figure 6C). We then examined the expression and phosphorylation status of the Lag1 protein in the Δtether and ypk1$^{ts}$ ypk2 mutant cells at 38°C by monitoring levels and mobility shifts of Lag1-GFP on Phos-tag acrylamide gels. First, steady-state expression levels of Lag1-GFP were reduced in the Δtether and ypk1$^{ts}$ ypk2 mutant cells (63 and 62% of wild-type levels respectively, normalized to a protein loading control; Figure 6D). Moreover, the Lag1-GFP protein was hypophosphorylated in the Δtether and ypk1$^{ts}$ ypk2 mutant cells (53 and 49% of wild-type levels, respectively; Figure 6, D and E). In these analyses, 14% of the total Lag1-GFP protein appeared as slower-migrating phosphorylated forms in wild-type cells (Figure 6E). However, in both Δtether and ypk1$^{ts}$ ypk2 mutant cells, approximately only 7% of the total Lag1-GFP protein was phosphorylated (Figure 6E). Lag1 is also phosphorylated by additional kinases, and this may explain the residual Lag1 phosphorylation observed in Δtether and ypk1$^{ts}$ ypk2 mutant cells (Fresques et al., 2015).
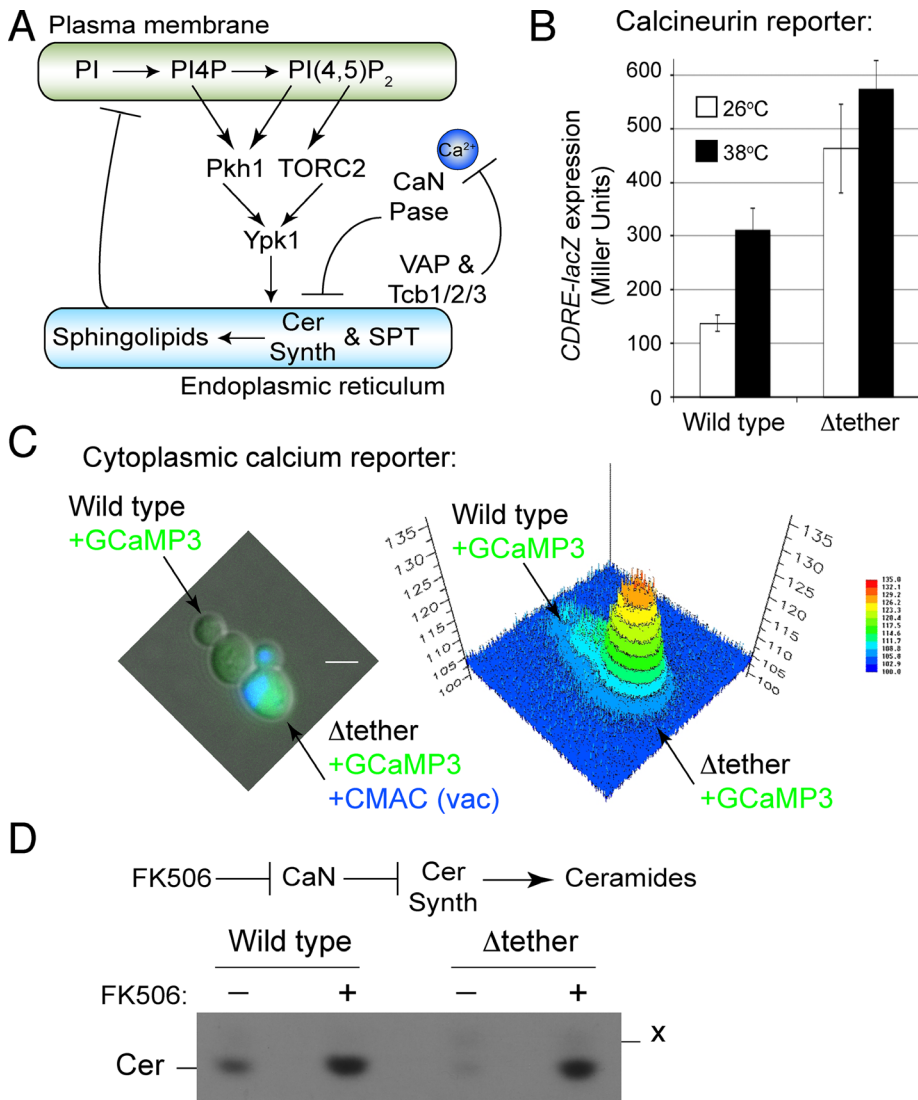
FIGURE 7: ER-PM junctions modulate cytoplasmic Ca²⁺ and calcineurin phosphatase activity during heat-induced ceramide synthesis. (A) Speculative model for a homeostatic regulatory loop in ER-PM cross-talk. Changes in membrane order and composition, including heat-induced membrane stress (Audhya and Emr, 2002) and other conditions, such as sphingolipid depletion (Jesch et al., 2010), increased PI kinase signaling up, regulating the Pkh1-TORC2-Ypk1 cascade. Ypk1 stimulates synthesis of LCBs and ceramides in the ER (via activation of serine palmitoyltransferase, SPT, and ceramide synthases) to adjust membrane lipid composition and protect PM integrity. The ER-localized Scs2/22 and Tcb1/2/3 proteins that form ER-PM junctions modulate cytoplasmic Ca²⁺ and calcineurin activity, which antagonizes sphingolipid synthesis in the ER. On restoration of membrane order, the PI kinase-Pkh1/2-TORC2-Ypk1/2 pathway is maintained at basal signaling levels. (B) Wild-type and Δtether cells carrying a *CDRE-lacZ* reporter were grown at 26°C and shifted to the indicated temperatures for 2 h, and β-galactosidase activity was determined. Data represent means ± SDs from three independent experiments. See Supplemental Figure S7A. (C) Wild-type and Δtether cells expressing cytoplasmic GCaMP3 were grown at 26°C. Vacuoles in Δtether cells were labeled with the dye CMAC to distinguish mutant cells from wild-type cells. Left, the cultures were mixed and simultaneously observed by fluorescence microscopy. Right, relative GCaMP3 intensities were quantified using soft-WoRx 3.5.0. Scale bar, 3 μm. See Supplemental Figure S7B. (D) Wild-type cells and Δtether cells were labeled with [³H]serine for 60 min at 26°C in the absence or presence of the calcineurin inhibitor FK506. Sphingolipids were extracted and analyzed by TLC. Ceramides (Cer) are indicated; an unknown lipid, X, was also observed.

The ER-localized ceramide synthases Lac1 and Lag1 could potentially be activated by the Ypk1/2 kinases at ER-PM junctions upon membrane stress. Indeed, localization of Lag1 in the cortical ER

increased upon heat stress (Supplemental Figure S6C). However Stt4, Mss4, Pkh1/2, and Ypk1/2 activities were not required for heat-induced localization of Lag1 to the cortical ER (unpublished data). Moreover, Lac1 localized to the nuclear ER even under membrane stress conditions (unpublished data), and both Lag1 and Lac1 were involved in maintaining PM integrity upon heat shock (Supplemental Figure S6D). The latter results indicated that Ypk1/2 signaling must be transduced to ceramide synthases localized throughout the ER. For these reasons, we searched for additional roles for the ER-PM tether proteins in regulation of ceramide synthesis.

ER-PM contacts modulate Ca²⁺ dynamics (Stefan et al., 2013), and the Ca²⁺/calmodulin-activated phosphatase calcineurin inhibits ceramide synthesis in the ER (Aronova et al., 2008; Muir et al., 2014; Figure 7A). We addressed whether misregulation of Ca²⁺ and calcineurin might impair ceramide synthesis in the Δtether cells. Basal expression of *CDRE::lacZ*, a reporter of calcineurin activity via its substrate the Crz1 transcription factor, was increased in the Δtether mutant cells fourfold above control levels (Figure 7B). Basal calcineurin activity in the Δtether cells was even greater than heat stress-induced levels in wild-type cells (Figure 7B). As further evidence for increased calcineurin activity, the Δtether mutant cells displayed resistance to the calcineurin inhibitor FK506 (Supplemental Figure S7A). Cells lacking either the VAPs or the tricalbin proteins were also resistant to FK506, specifically implicating these tether proteins in the control of calcineurin and cellular Ca²⁺ levels (Supplemental Figure S7A). Consistent with this, fluorescence of the cytoplasmic Ca²⁺ reporter GCaMP3 was increased in Δtether cells as compared with wild-type cells (approximately threefold by fluorescence microscopy; Figure 7C). In high-content quantitative flow cytometry assays, the GCaMP3 signal doubled in Δtether cells compared with wild type (Supplemental Figure S7B). Cytoplasmic Ca²⁺ was not significantly elevated in *sac1Δ* cells (Supplemental Figure S7B), suggesting that elevated PI4P or LCBs may not activate calcineurin in the Δtether cells. Thus the ER-PM tether proteins function to modulate cellular Ca²⁺ levels and calcineurin activity. Of interest, the calcineurin inhibitor FK506 increased ceramide production in the Δtether cells (Figure 7D), suggesting that increased calcineurin activity was at least partially re-

sponsible for the impaired Lac1/Lag1 function and sphingolipid synthesis defects observed in these cells. Overall our results suggest that PI kinase-Pkh1/2-TORC2 signaling controls ER-PM cross-talk

during membrane stress conditions and that ER-PM junctions modulate cytoplasmic $Ca^{2+}$ levels and calcineurin activity, which antagonizes sphingolipid synthesis in the ER (Figure 7A).

## DISCUSSION

### PI kinase signaling controls PM homeostasis

We propose that PI kinase signaling controls ER-PM cross-talk necessary for cellular integrity and membrane homeostasis. We identify the PDK orthologue Pkh1 as an effector of Stt4 and Mss4 PI kinase activities at the PM (Figure 3). PI4P and $PI(4,5)P_2$ may recruit Pkh1 to the PM upon heat-induced membrane stress, as cortical Pkh1 assemblies constitutively formed in mutant cells with elevated PI4P and $PI(4,5)P_2$ levels (Figure 4 and Supplemental Table S3). Thus PI kinases may regulate both Pkh1/2 and TORC2 at the PM, where they phosphorylate the Akt orthologues Ypk1/2. Our study and previous work (Muir *et al.*, 2014) indicate that Ypk1/2 subsequently activate ceramide synthases localized in the ER for de novo sphingolipid synthesis essential for cellular integrity upon stress conditions. Of interest, control of ceramide synthesis by PDK-Akt-mTor signaling may be conserved. A large-scale proteomic study identified several mammalian ceramide synthase isoforms as targets of the PI3K-PDK-Akt-mTor signaling pathway (Humphrey *et al.*, 2013).

The Mss4 PI4P 5-kinase and $PI(4,5)P_2$ are critical regulators of Pkh1 and TORC2 signaling (Figures 3 and 5). However, our data suggest that PI4P may also recruit Pkh1 to the PM. Why, then, might yeast cells have redundant mechanisms in place for Pkh1 regulation? On certain membrane stress conditions, including sphingolipid depletion, PI4P signaling may provide important contributions to Ypk1-mediated lipid synthesis in the ER. Sphingolipids are suggested to modulate Mss4 localization and thus $PI(4,5)P_2$ synthesis (Kobayashi *et al.*, 2005; Gallego *et al.*, 2010). PI4P availability is increased at the PM upon inhibition of sphingolipid synthesis (Jesch *et al.*, 2010), and PI4P may provide a protective mechanism that sustains or even triggers Pkh1-TORC2-Ypk1 signaling upon compromised sphingolipid and $PI(4,5)P_2$ production. As such, both PI4P and $PI(4,5)P_2$ may provide important regulatory inputs for the modulation of Ypk1 signaling and ER-PM cross-talk.

### The calcium paradox in cellular stress responses

Cytoplasmic $Ca^{2+}$ and calcineurin activity increase upon heat-induced membrane stress (Figure 7B; Cunningham, 2011), possibly to regulate endocytosis (Wu *et al.*, 2014) for the clearance of damaged PM proteins (Zhao *et al.*, 2013). However, calcineurin inhibits sphingolipid synthesis, which is also essential for cellular integrity upon heat stress (Figures 2 and 7 and Supplemental Figure S6E; Aronova *et al.*, 2008; Muir *et al.*, 2014). Cells may overcome this paradox in $Ca^{2+}$ stress responses through the formation of ER-PM junctions. The PM is organized into distinct functional domains, including ER-free zones and ER-associated PM zones. $Ca^{2+}$- and calcineurin-mediated endocytosis takes place in the ER-free PM zones (Stradalova *et al.*, 2012). ER-PM junctions may serve as sites to modulate cytoplasmic $Ca^{2+}$ signals and calcineurin. In line with this, the Δtether cells display elevated cytoplasmic $Ca^{2+}$ and calcineurin activity (Figure 7). How the ER-PM tether proteins regulate $Ca^{2+}$ dynamics is unclear. Similarly, the source of increased $Ca^{2+}$ in the Δtether cells is unknown (i.e., extracellular or intracellular stores). However, the tricalbin proteins (E-Syt orthologues) possess $Ca^{2+}$-binding C2 domains and may be activated by $Ca^{2+}$ for feedback regulation of $Ca^{2+}$ flux into the cytoplasm. Accordingly, loss of the tricalbins resulted in increased calcineurin activity (Supplemental Figure S7) and cell integrity defects upon heat shock (Supplemental Figure S1). Consis-

tent with this, mammalian E-Syt proteins are regulated by the store-operated $Ca^{2+}$ entry (SOCE) pathway and subsequently inactivate SOCE (Giordano *et al.*, 2013; Maleth *et al.*, 2014; Idevall-Hagren *et al.*, 2015). Moreover, ER-PM junctions are sites for inhibition of voltage-gated $Ca^{2+}$ channels (VGCCs; Park *et al.*, 2010; Wang *et al.*, 2010), but the E-Syt proteins have yet to be implicated in VGCC regulation.

### Sphingolipid signaling in membrane stress responses

Cells up-regulate sphingolipid synthesis in the ER in response to heat-induced membrane stress (Figure 2; Tabuchi *et al.*, 2006; Sun *et al.*, 2012; Muir *et al.*, 2014). Increased production of LCBs and ceramides induce several heat stress responses, including transcription of heat stress genes, translation of heat shock factors and chaperones, and membrane trafficking (Cowart and Obeid, 2007). Our results indicate that PI kinase–stimulated sphingolipid synthesis in the ER is critical for maintaining PM integrity—but are specialized pools of sphingolipids generated, how are they delivered to the PM, and what are their protective roles during PM stress?

Of interest, the Orm2 protein that inhibits LCB synthesis is depleted from the cortical ER upon membrane stress, whereas the Lag1 ceramide synthesis moves into the cortical ER (Breslow *et al.*, 2010; Supplemental Figure S6). Possibly, localized pools of LCBs and ceramides are generated in the cortical ER at PM contact zones, where they may regulate stress response mechanisms such as a LCB- or ceramide-activated protein kinase or phosphatase. Intriguingly, the PH domain from the Slm1 protein possesses distinct sites that bind PI4P and LCBs (Anand *et al.*, 2012). Our results indicate that basal TORC2 signaling is increased in *sac1* and Δtether mutant cells, which have elevated levels of PI4P and LCBs (Figures 5B and 6A; Manford *et al.*, 2012), suggesting that PI4P-regulated sphingolipid synthesis might function in a feedforward regulatory loop to control TORC2 signaling and sphingolipid synthesis.

ER-PM junctions are sites for nonvesicular transport where lipid transfer proteins use PI metabolism for membrane lipid delivery (Moser von Filseck *et al.*, 2014). Possibly, LCBs or ceramides generated in the cortical ER are shuttled to the PM by an unidentified lipid transfer protein to provide structural support or maintain lipid-packing order in the PM. Long-acyl-chain lipids, including sphingolipids, are also proposed to serve as a "chemical trap" for sterol lipids that could effectively reduce PM permeability (Holthuis and Menon, 2014). Increased sphingolipid content may also create a membrane environment that favors the proper folding and thermostability of integral PM proteins at elevated temperatures. We do not have a full understanding of how PI kinase signaling controls PM organization and integrity. However, PI kinase–regulated ER-PM cross-talk provides an elegant mechanism to coordinate both the synthesis and traffic of membrane lipids.

Ceramides are transported from the ER by both nonvesicular and vesicular membrane trafficking pathways (Funato and Riezman, 2001). PI kinase–regulated sphingolipid synthesis may be vital for essential functions of the ER as well, including folding and secretion of newly synthesized proteins such as thermoresistant PM proteins. Accordingly, sphingolipids are involved in the ER export and targeting of integral PM proteins, including the yeast PM ATPase Pma1 and the nutrient permeases Can1 and Gap1 (Lee *et al.*, 2002; Wang and Chang, 2002; Daquinag *et al.*, 2007; Lauwers *et al.*, 2007). Consequently, impaired ceramide synthesis in cells lacking ER-PM tether proteins could lead to cargo-specific ER export defects that may contribute to ER stress phenotypes previously observed in Δtether cells (Manford *et al.*, 2012).

We propose that PI kinase-Pkh1-TORC2 signaling is part of an essential pathway for membrane homeostasis. Of interest, upon loss of the ER tether proteins, additional cellular stress response pathways are activated, including the unfolded protein response in the ER (Manford et al., 2012), a mitogen-activated protein kinase (MAPK)–regulated cell integrity pathway (Figure 5), and calcineurin-mediated transcriptional responses (Figure 7), potentially to compensate for loss of ER-PM crosstalk. Thus PI kinase signaling may coordinately regulate ER-PM cross-talk and other stress response pathways to maintain membrane homeostasis and cellular integrity. It will be important to investigate further how ER-PM cross-talk affects PDK-Akt-mTor signaling and other stress responses in the control of membrane organization.

## MATERIALS AND METHODS
Additional details are provided in the Supplemental Materials and Methods.

### Strains and plasmids
Strains and plasmids used in this study are listed in Supplemental Tables S1 and S2, respectively.

### Fluorescence microscopy
Images were obtained with a DeltaVision RT microscopy system (GE Applied Precision, Issaquah, WA) or spinning-disk confocal microscopy systems (Perkin Elmer, Waltham, MA, and 3i, Denver, CO). See Supplemental Materials and Methods for additional microscopy details.

### Plasma membrane integrity assays
PM integrity assays were performed as described (Zhao et al., 2013). Cells were grown at 26°C and shifted to 40°C for 2 h (heat stress conditions) or to 42°C for 10–15 min (heat shock) as indicated. Cells were stained with propidium iodide, washed, and analyzed by flow cytometry. See the Supplemental Materials and Methods for additional details.

### Sphingolipid analysis
Metabolic labeling, lipid extraction, and TLC analysis of sphingolipids were performed as described (Tabuchi et al., 2006). See the Supplemental Materials and Methods for additional sphingolipid analysis details.

### Analysis of protein phosphorylation and expression
Cells were mechanically lysed in the presence of phosphatase inhibitors. Extracts were analyzed by SDS–PAGE and immunoblotting with the following antibodies: anti-Pep12 (Invitrogen, Thermo Fisher Scientific, Waltham, MA), anti–glucose-6-phosphate dehydrogenase (G6PDH; Sigma-Aldrich, St. Louis, MO), anti–phosphoglycerate kinase (PGK; Novex, Thermo Fisher Scientific, Waltham, MA), anti-GFP (Santa Cruz Biotechnology, Dallas, TX, or Roche, Burgess Hill, UK), anti-PKC (pan) zeta T410 (Cell Signaling, Danvers, MA) for phospho-Ypk1(T504), anti-phospho-Ypk1(T662) (Niles et al., 2012), anti-Ypk1 (Cell Signaling), and anti–phospho-p44/42 MAPK (Cell Signaling) for phospho-Slt2. Levels of GFP-Pkh1, Ypk1, phospho-Ypk1, and phospho-Slt2 were normalized to protein loading controls (Pep12, G6PDH, or PGK). See the Supplemental Materials and Methods for additional details.

### β-Galactosidase assays
Strains harboring a *CDRE-lacZ* reporter were grown at 26°C, and indicated samples were shifted to 38°C for 2 h. β-Galactosidase activity was measured as described in the Supplemental Materials and Methods.

### Quantitative GCaMP3 fluorescence assays
Strains harboring a cytoplasmic GCaMP3 reporter were grown at 26°C and transferred to phosphate-buffered saline. Mean fluorescence of 50,000 events was recorded on a BD Accuri C6 flow cytometer. Background was determined using strains harboring vector alone. Results are the mean of three independent experiments. See the Supplemental Materials and Methods for additional details.

## REFERENCES
Anand K, Maeda K, Gavin AC (2012). Structural analyses of the Slm1-PH domain demonstrate ligand binding in the non-canonical site. PLoS One 7, e36526.

Aronova S, Wedaman K, Aronov PA, Fontes K, Ramos K, Hammock BD, Powers T (2008). Regulation of ceramide biosynthesis by TOR complex 2. Cell Metab 7, 148–158.

Audhya A, Emr SD (2002). Stt4 PI 4-kinase localizes to the plasma membrane and functions in the Pkc1-mediated MAP kinase cascade. Dev Cell 2, 593–605.

Audhya A, Foti M, Emr SD (2000). Distinct roles for the yeast phosphatidylinositol 4-kinases, Stt4p and Pik1p, in secretion, cell growth, and organelle membrane dynamics. Mol Biol Cell 11, 2673–2689.

Audhya A, Loewith R, Parsons AB, Gao L, Tabuchi M, Zhou H, Boone C, Hall MN, Emr SD (2004). Genome-wide lethality screen identifies new PI4,5P2 effectors that regulate the actin cytoskeleton. EMBO J 23, 3747–3757.

Berchtold D, Piccolis M, Chiaruttini N, Riezman I, Riezman H, Roux A, Walther TC, Loewith R (2012). Plasma membrane stress induces relocalization of Slm proteins and activation of TORC2 to promote sphingolipid synthesis. Nat Cell Biol 14, 542–547.

Breslow DK, Collins SR, Bodenmiller B, Aebersold R, Simons K, Shevchenko A, Ejsing CS, Weissman JS (2010). Orm family proteins mediate sphingolipid homeostasis. Nature 463, 1048–1053.

Brice SE, Alford CW, Cowart LA (2009). Modulation of sphingolipid metabolism by the phosphatidylinositol-4-phosphate phosphatase Sac1p through regulation of phosphatidylinositol in Saccharomyces cerevisiae. J Biol Chem 284, 7588–7596.

Cowart LA, Hannun YA (2007). Selective substrate supply in the regulation of yeast de novo sphingolipid synthesis. J Biol Chem 282, 12330–12340.

Cowart LA, Obeid LM (2007). Yeast sphingolipids: recent developments in understanding biosynthesis, regulation, and function. Biochim Biophys Acta 1771, 421–431.

Cunningham KW (2011). Acidic calcium stores of Saccharomyces cerevisiae. Cell Calcium 50, 129–138.

Daquinag A, Fadri M, Jung SY, Qin J, Kunz J (2007). The yeast PH domain proteins Slm1 and Slm2 are targets of sphingolipid signaling during the response to heat stress. Mol Cell Biol 27, 633–650.

Fresques T, Niles B, Aronova S, Mogri H, Rakhshandehroo T, Powers T (2015). Regulation of ceramide synthase by casein kinase 2-dependent phosphorylation in Saccharomyces cerevisiae. J Biol Chem 290, 1395–1403.

Friedman JR, Voeltz GK (2011). The ER in 3D: a multifunctional dynamic membrane network. Trends Cell Biol 21, 709–717.

Funato K, Riezman H (2001). Vesicular and nonvesicular transport of ceramide from ER to the Golgi apparatus in yeast. J Cell Biol 155, 949–959.

Gallego O, Betts MJ, Gvozdenovic-Jeremic J, Maeda K, Matetzki C, Aguilar-Gurrieri C, Beltran-Alvarez P, Bonn S, Fernandez-Tornero C, Jensen LJ, et al. (2010). A systematic screen for protein-lipid interactions in Saccharomyces cerevisiae. Mol Syst Biol 6, 430.

Giordano F, Saheki Y, Idevall-Hagren O, Colombo SF, Pirruccello M, Milosevic I, Gracheva EO, Bagriantsev SN, Borgese N, De Camilli P (2013). PI(4,5) P(2)-dependent and Ca(2+)-regulated ER-PM interactions mediated by the extended synaptotagmins. Cell 153, 1494–1509.

Gururaj C, Federman R, Chang A (2013). Orm proteins integrate multiple signals to maintain sphingolipid homeostasis. J Biol Chem 288, 20453–20463.

Holthuis JC, Menon AK (2014). Lipid landscapes and pipelines in membrane homeostasis. Nature 510, 48–57.

Humphrey SJ, Yang G, Yang P, Fazakerley DJ, Stockli J, Yang JY, James DE (2013). Dynamic adipocyte phosphoproteome reveals that Akt directly regulates mTORC2. Cell Metab 17, 1009–1020.

Idevall-Hagren O, Lu A, Xie B, De Camilli P (2015). Triggered Ca2+ influx is required for extended synaptotagmin 1-induced ER-plasma membrane tethering. EMBO J 34, 2291–2305.

Jesch SA, Gaspar ML, Stefan CJ, Aregullin MA, Henry SA (2010). Interruption of inositol sphingolipid synthesis triggers Stt4p-dependent protein kinase C signaling. J Biol Chem 285, 41947–41960.

Kobayashi T, Takematsu H, Yamaji T, Hiramoto S, Kozutsumi Y (2005). Disturbance of sphingolipid biosynthesis abrogates the signaling of Mss4, phosphatidylinositol-4-phosphate 5-kinase, in yeast. J Biol Chem 280, 18087–18094.

Lauwers E, Grossmann G, Andre B (2007). Evidence for coupled biogenesis of yeast Gap1 permease and sphingolipids: essential role in transport activity and normal control by ubiquitination. Mol Biol Cell 18, 3068–3080.

Lee MC, Hamamoto S, Schekman R (2002). Ceramide biosynthesis is required for the formation of the oligomeric H+-ATPase Pma1p in the yeast endoplasmic reticulum. J Biol Chem 277, 22395–22401.

Liu K, Zhang X, Lester RL, Dickson RC (2005). The sphingoid long chain base phytosphingosine activates AGC-type protein kinases in Saccharomyces cerevisiae including Ypk1, Ypk2, and Sch9. J Biol Chem 280, 22679–22687.

Maleth J, Choi S, Muallem S, Ahuja M (2014). Translocation between PI(4,5) P2-poor and PI(4,5)P2-rich microdomains during store depletion determines STIM1 conformation and Orai1 gating. Nat Commun 5, 5843.

Manford AG, Stefan CJ, Yuan HL, Macgurn JA, Emr SD (2012). ER-to-plasma membrane tethering proteins regulate cell signaling and ER morphology. Dev Cell 23, 1129–1140.

Moser von Filseck J, Mesmin B, Bigay J, Antonny B, Drin G (2014). Building lipid "PIPelines" throughout the cell by ORP/Osh proteins. Biochem Soc Trans 42, 1465–1470.

Muir A, Ramachandran S, Roelants FM, Timmons G, Thorner J (2014). TORC2-dependent protein kinase Ypk1 phosphorylates ceramide synthase to stimulate synthesis of complex sphingolipids. eLife 3, doi: 10.7554/eLife.03779.

Niles BJ, Mogri H, Hill A, Vlahakis A, Powers T (2012). Plasma membrane recruitment and activation of the AGC kinase Ypk1 is mediated by target of rapamycin complex 2 (TORC2) and its effector proteins Slm1 and Slm2. Proc Natl Acad Sci USA 109, 1536–1541.

Park CY, Shcheglovitov A, Dolmetsch R (2010). The CRAC channel activator STIM1 binds and inhibits L-type voltage-gated calcium channels. Science 330, 101–105.

Roelants FM, Breslow DK, Muir A, Weissman JS, Thorner J (2011). Protein kinase Ypk1 phosphorylates regulatory proteins Orm1 and Orm2 to control sphingolipid homeostasis in Saccharomyces cerevisiae. Proc Natl Acad Sci USA 108, 19222–19227.

Roelants FM, Torrance PD, Thorner J (2004). Differential roles of PDK1- and PDK2-phosphorylation sites in the yeast AGC kinases Ypk1, Pkc1 and Sch9. Microbiology 150, 3289–3304.

Stefan CJ, Manford AG, Emr SD (2013). ER-PM connections: sites of information transfer and inter-organelle communication. Curr Opin Cell Biol 25, 434–442.

Stradalova V, Blazikova M, Grossmann G, Opekarova M, Tanner W, Malinsky J (2012). Distribution of cortical endoplasmic reticulum determines positioning of endocytic events in yeast plasma membrane. PLoS One 7, e35132.

Sun Y, Miao Y, Yamane Y, Zhang C, Shokat KM, Takematsu H, Kozutsumi Y, Drubin DG (2012). Orm protein phosphoregulation mediates transient sphingolipid biosynthesis response to heat stress via the Pkh-Ypk and Cdc55-PP2A pathways. Mol Biol Cell 23, 2388–2398.

Tabuchi M, Audhya A, Parsons AB, Boone C, Emr SD (2006). The phosphatidylinositol 4,5-biphosphate and TORC2 binding proteins Slm1 and Slm2 function in sphingolipid regulation. Mol Cell Biol 26, 5861–5875.

Wang Q, Chang A (2002). Sphingoid base synthesis is required for oligomerization and cell surface stability of the yeast plasma membrane ATPase, Pma1. Proc Natl Acad Sci USA 99, 12853–12858.

Wang Y, Deng X, Mancarella S, Hendron E, Eguchi S, Soboloff J, Tang XD, Gill DL (2010). The calcium store sensor, STIM1, reciprocally controls Orai and CaV1.2 channels. Science 330, 105–109.

Wu XS, Zhang Z, Zhao WD, Wang D, Luo F, Wu LG (2014). Calcineurin is universally involved in vesicle endocytosis at neuronal and nonneuronal secretory cells. Cell Rep 7, 982–988.

Zhao Y, Macgurn JA, Liu M, Emr S (2013). The ART-Rsp5 ubiquitin ligase network comprises a plasma membrane quality control system that protects yeast cells from proteotoxic stress. eLife 2, e00459.

# Supplemental Materials

*Molecular Biology of the Cell*

Omnus et al.

# Supplemental Information

## PI 4-Kinase Signaling Controls ER-PM Crosstalk

Deike J. Omnus, Andrew G. Manford,,JakobM. Bader,Scott D. Emr, and Christopher J. Stefan

The Supplemental Information includes sevenfigures, figure and movie legends, 2 movies,3 tables, supplemental materials and methods, and references.

Figure S1, related to Figure 1C. PM integrity of wild type, Δtether,*scs2/22Δ*, *tcb1/2/3Δ*, and *ist2Δ* cells upon brief heat shock.

Figure S2, related to Figure 2. ER-PM junctions regulate sphingolipid synthesis.

Figure S3, related to Figures3A and 3B. PI metabolism regulates Pkh1 signaling.

Figure S4, related to Figure 4. PI metabolismregulates Pkh1 localization.

Figure S5, related to Figure 5. TORC2 signaling is elevated upon loss of Pkh1/2 function.

Figure S6, related to Figure 6. ER-PM junctions control ceramide synthase activity in the ER.

Figure S7, related to Figure7. ER-PM junctions modulate cytoplasmic $Ca^{2+}$ and calcineurin phosphatase activity.

Table S1. Related to Materials and Methods. Strains used in this study.

Table S2. Related to Materials and Methods. Plasmids used in this study.

Table S3.GFP-Pkh1 localization upon changes in PI lipids and sphingolipids.

Supplemental Figure Legends

SupplementalMaterials and Methods

SupplementalReferences

MoviesS1 and S2.

A

PM Integrity Assay (rich media):

B

PM Integrity Assay
(selective media):

C

mCh-2xPH^PLCδ-Scs2^129-244        Sec61-GFP        merge

D

Wild type        Δtether

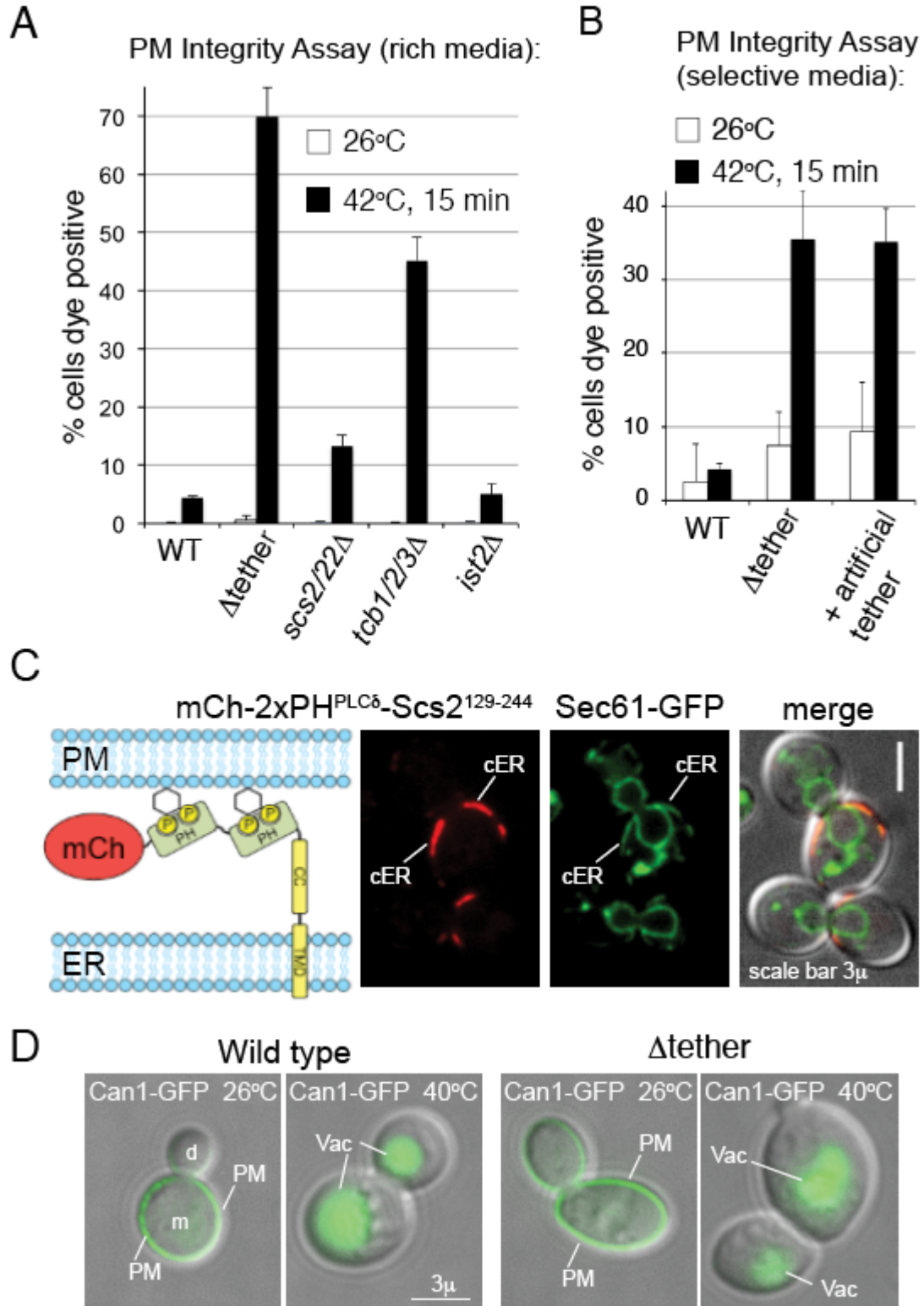**Figure S1, related to Figure 1C. PM integrity of wild type, Δtether, *scs2/22Δ*, *tcb1/2/3Δ*, and *ist2Δ* cells upon brief heat shock.**

A Propidium iodide PM integrity assays on cells grown in rich YPD media incubated at 26°C (white) or following a brief heat shock at 42°C for 10 min (black). Flow cytometry was used to analyze propidium iodide staining.

B Propidium iodide PM integrity assays on Δtether cells expressing the artificial ER-PM tether 2xPH$^{PLC\delta}$-Scs2$^{129-244}$ compared to control wild type cells and Δtether cells carrying empty vector. Cells grown in selective media either incubated at 26°C (white) or exposed to a brief heatshock at 42°C for 10 minutes (black) were analyzed by flow cytometry to monitor propidium iodide staining.

C The chimeric protein mCherry-2xPH$^{PLC\delta}$-Scs2$^{129-244}$ forms cortical ER in Δtether cells co-expressing Sec61-GFP as an ER marker. A schematic diagram of the artificial chimeric ER-PM tether is shown (left panel). Scale bar, 3 μm.

D Distribution of the endocytic cargo protein Can1-GFP was analyzed in wild type cells and Δtether cells. Cells were grown to mid-log at 26°C and then shifted to 40°C for 2 hours. Plasma membrane (PM) and vacuole (Vac) localization are indicated. Scale bar, 3μm.
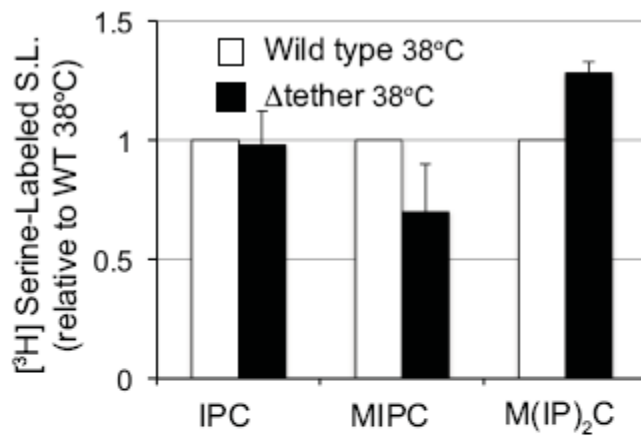
# Omnus *et al.*, Figure S2

## A

Sphingolipid Synthesis 26°C:



## B
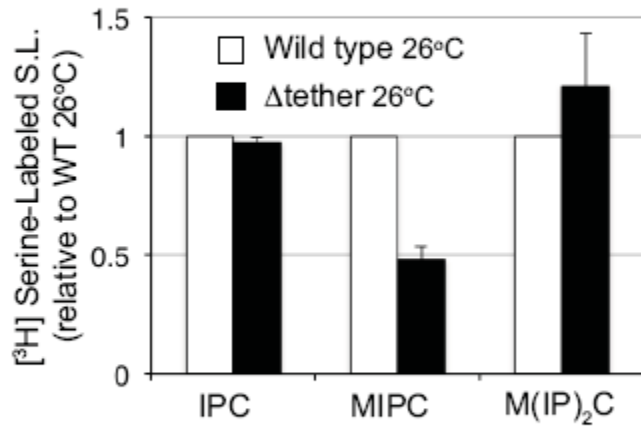
Sphingolipid Synthesis 38°C:



## C

AurA halos:

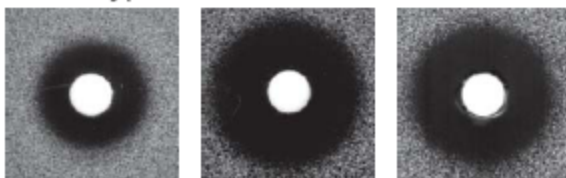| Wild type | Δtether | Δtether + A.T. |

**Figure S2, related to Figure 2.ER-PM junctions regulate sphingolipid synthesis in the ER.**

A  Quantitation ofcomplex sphingolipid species IPC, MIPC, and M(IP)$_2$C synthesis in $\Delta$tether cells normalized to wild type levels at 26$^o$C. The data represent the means ± standard deviations from three independent experiments. See Figure 2 and Supplemental Materials and Methods for further details on sphingolipid analysis.

B  Quantitation of complex sphingolipid species IPC, MIPC, and M(IP)$_2$C synthesis in $\Delta$tether cells normalized to wild type levels at 38$^o$C (heat stress conditions). The data represent the means ± standard deviations from three independent experiments. See Figure 2 and Supplemental Materials and Methods for further details on sphingolipid analysis.

CWild type cells carrying vector alone,$\Delta$tether cells carrying vector alone, and $\Delta$tether cells carrying a plasmid expressing the artificial tether protein 2xPH$^{PLC\delta}$-Scs2$^{129-244}$ (+A.T.) were plated as lawns and then overlaid with sterile filter discs containing 10 $\mu$l of a 1 mg/ml stock of aureobasidin A (AurA) in DMSO. After incubation at 26°C for 3 days, the plates were imaged. Wild type cells form a zone of growth inhibition (halos). The $\Delta$tether cells display hypersensitivity to AurA as indicated by increased halo diameter. Expression of the artificial tether (+A.T.) did not rescue the AurA hypersensitivity of the $\Delta$tethercells.
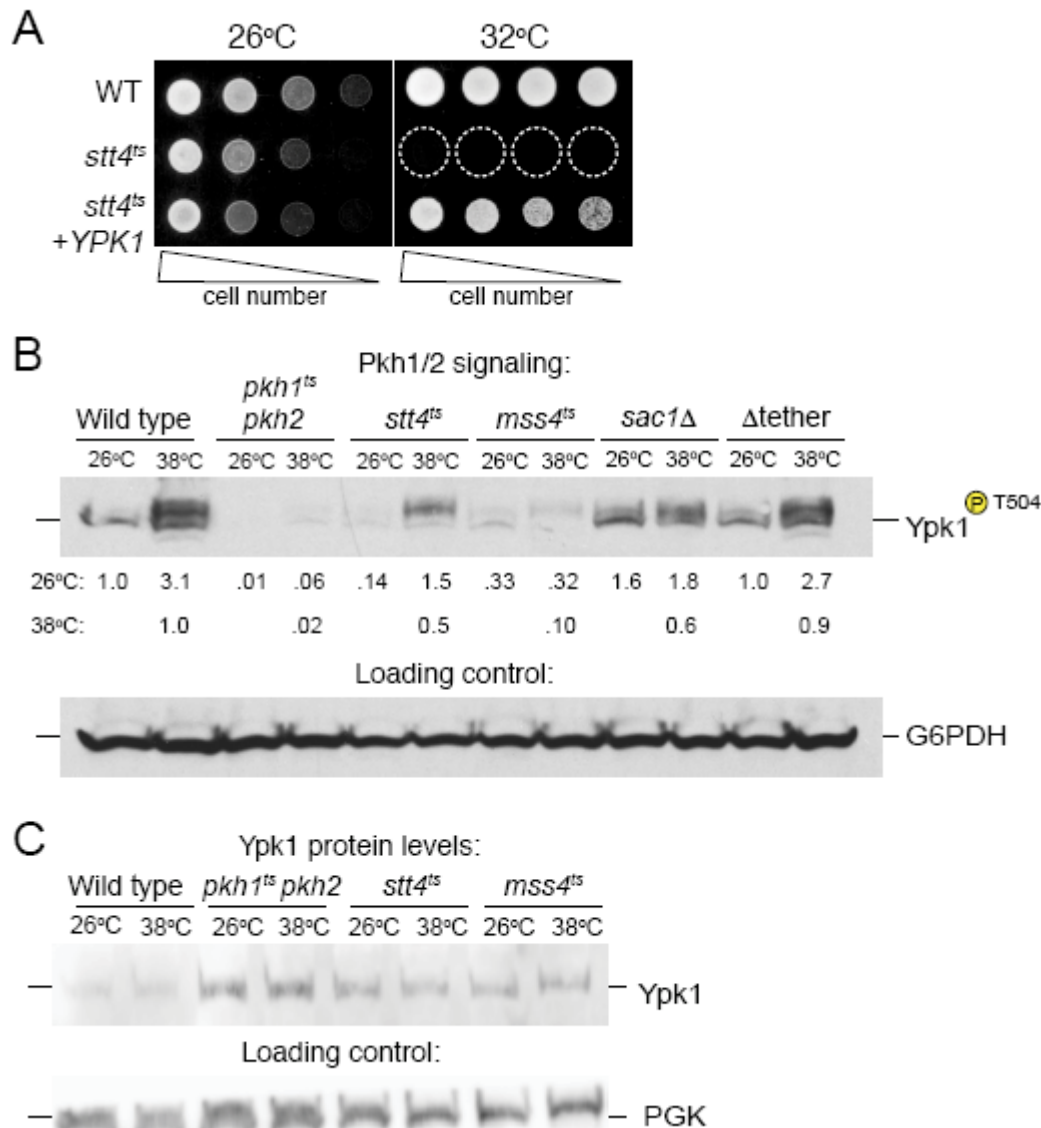
## Omnus *et al.*, Figure S3



**Figure S3, related to Figure 3. PI kinase signaling regulates Pkh1.**

A  Ypk1 overexpression rescues the growth defects of *stt4$^{ts}$* cells. Serial dilutions of wildtype and *stt4$^{ts}$* cells carrying vector or a plasmid overexpressing *YPK1* from the *MET25* promoter were spotted on media lacking methionine at the indicated temperatures.

B Analysis of Pkh1/2 signaling in wild type, *pkh1$^{ts}$pkh2Δ*, *stt4$^{ts}$*, *mss4$^{ts}$*, *sac1Δ*, and Δtether cells. Cells were incubated at 26°C or 38°C for 2 hours. Protein extracts were analyzed by immunoblotting using antisera that recognize phospho-Ypk1(T504). Levels of a protein loading control (G6PDH) are also shown. Quantifications below the blot report the difference relative to WT after normalizing to the protein loading control; results shown here are from a single

representative experiment.See Figure 3B for the quantitation of results (normalized to the protein loading control) from three independent experiments.

C  Analysis of Ypk1 protein levels in wildtype, *pkh1$^{ts}$pkh2Δ*, *stt4$^{ts}$*, and *mss4$^{ts}$* cells incubated at 26°C or 38°C for 2 hours. Protein extracts were analyzed by immunoblotting using antisera that recognize Ypk1 or a protein loading control (PGK). Results from a single experiment are shown. Levels of Ypk1 (normalized to the protein loading control) in *pkh1$^{ts}$pkh2Δ*, *stt4$^{ts}$*, and *mss4$^{ts}$* cells were 2.3-fold, 1.3-fold, and 1.8-fold greater than wildtype levels at 38°C, as determined from two independent experiments.

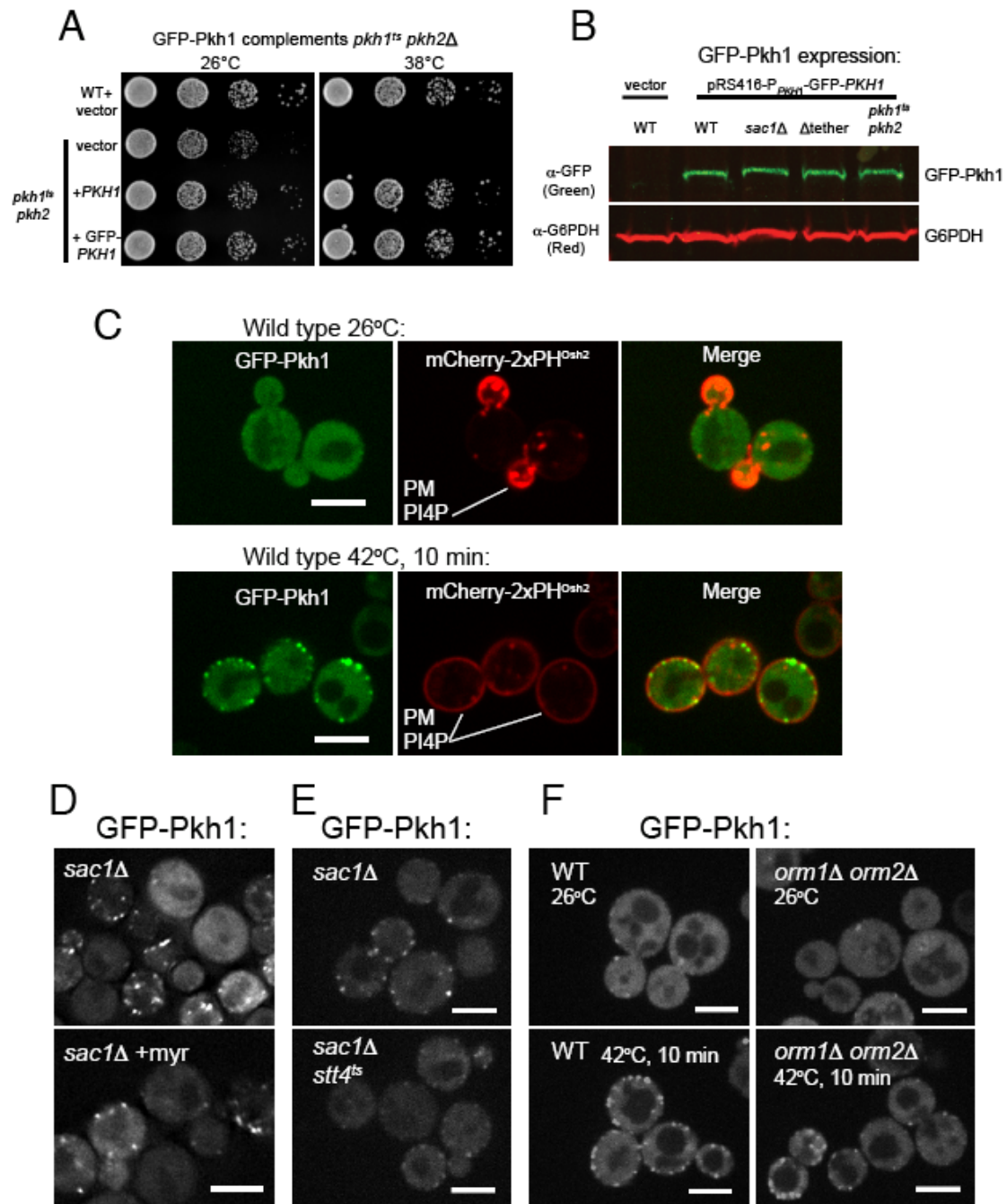

**Figure S4, related to Figure 4. PI kinase signaling regulates Pkh1 localization.**

AThe GFP-Pkh1 fusion is functional. Serial dilutions of wild type and *pkh1^{ts}pkh2Δ* double mutant cells carrying vector alone or a centromeric plasmid expressing *PKH1* or *GFP-PKH1* from the *PKH1* promoter were incubated at the indicated

temperatures. Expression of Pkh1 or GFP-Pkh1 rescues the growth defects of *pkh1$^{ts}$pkh2Δ* double mutant cells at the restrictive temperature.

BSteady-state GFP-Pkh1 expression levels in wild type, *sac1Δ*, Δtether, and *pkh1$^{ts}$pkh2Δ* double mutant cells carrying a centromeric*GFP-PKH1* expression vector were grown at 26°C. GFP-Pkh1 expression levels are similar in lysates from wild type and all the mutant cells, as analyzed by immunoblotting using GFP antibodies. G6PDH is used as a loading control. Wild type cells carrying empty vector were followed as a control for the GFP antisera.

C  Pkh1 assembles at ER-associated cortical patches upon heat shock. Wildtype cells expressing GFP-Pkh1 and the PI4P reportermCherry-2xPH$^{Osh2}$ were grown at 26$^{o}$C (top) and shifted to 42$^{o}$C for 10 min (bottom). The majority of GFP-Pkh1 foci are cortical, but internal patches are also observed.Scale bar, 5μm.

D  GFP-Pkh1 localization in *sac1Δ*cells at 26$^{o}$C in the absence of (top panel) or following treatment with the SPT inhibitor myriocin (bottom panel). GFP-Pkh1 puncta are found in myriocin-treated *sac1Δ*cells, suggesting that recruitment of Pkh1 does not require continued synthesis of long chain sphingoid bases (LCBs). The number of puncta per cell for both conditions (in single focal planes) was quantified using ImageJ(Fiji) (see Table S3).Scale bar, 5μm.

E  PI4P metabolism controls Pkh1 localization, as assessed by formation of GFP-Pkh1 assemblies in *sac1Δ* and *stt4$^{ts}$ sac1Δ* cells. The assembly of GFP-Pkh1 puncta was reduced in*stt4$^{ts}$ sac1Δ*cells as compared to*sac1Δ* cells as indicated by quantitative analysis using ImageJ (Fiji).The number of GFP-Pkh1 foci per cell identified above a high threshold intensity value (noise tolerance=2400) decreased two-fold in *stt4$^{ts}$ sac1Δ* double mutant cells (n=1007 foci in 935 cells) as compared to *sac1Δ* single mutant cells (n=1430 foci in 682 cells).Scale bar, 5μm.

F GFP-Pkh1 localization in wild type and *orm1Δorm2Δ* cells grown at 26$^{o}$C (top) and shifted to 42$^{o}$C for 10 min (bottom) prior to image acquisition. GFP-Pkh1 foci were not increased in *orm1Δorm2Δ* cells as compared to wildtype, suggesting elevated LCBs are not sufficient for Pkh1 membrane recruitment.The number of puncta per cell (in single focal planes) was quantified using ImageJ (Fiji) (see Table S3).Scale bar, 5μm.
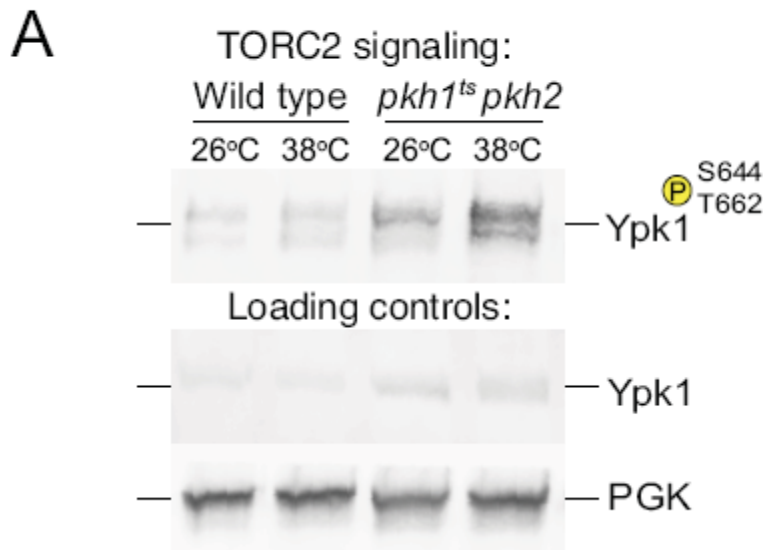
# Omnus *et al.*, Figure S5

## A



TORC2 signaling:

Wild type    *pkh1$^{ts}$ pkh2*

26°C   38°C    26°C   38°C

Ypk1 $\quad$ S644 / T662 (P)

Loading controls:

Ypk1

PGK

**Figure S5, related to Figure 5. Sphingolipid metabolism controls TORC2 signaling.**

TORC2 signaling is increased in *pkh1$^{ts}$ pkh2*Δcells. Wildtype and *pkh1$^{ts}$ pkh2*Δcells were incubated at 26°C or 38°C for 2 hours. Protein extracts were prepared, loaded onto SDS-PAGE gels, and analyzed by immunoblotting using antisera that specifically recognize phospho-Ypk1(T662) (Niles *et al.*, 2012)or Ypk1 (Cell Signaling). Upon loss of Pkh1/2 function at 38°C, phospho-Ypk1(T662) levels were increased 6-fold above wildtype levels at 38°C (normalized to the PGK protein loading control). Ypk1 protein levels (normalized to the PGK protein loading control) were also increased 2.3-fold in *pkh1$^{ts}$ pkh2*Δcells compared to wildtype control cells (also see Figure S3C). However, this does fully account for the increase in phospho-Ypk1(T662) levels.

A  myriocin halos assays:

Wild type    Δtether



B  myriocin halos assays:

Wild type    Δtether    Δtether
+ vector    + vector    + artificial tether



C

Wild type cells 26°C

Lag1-GFP    cER    merge/DIC
cER
n    n
cER    26°C

Wild type cells 38°C

Lag1-GFP    cER    merge/DIC
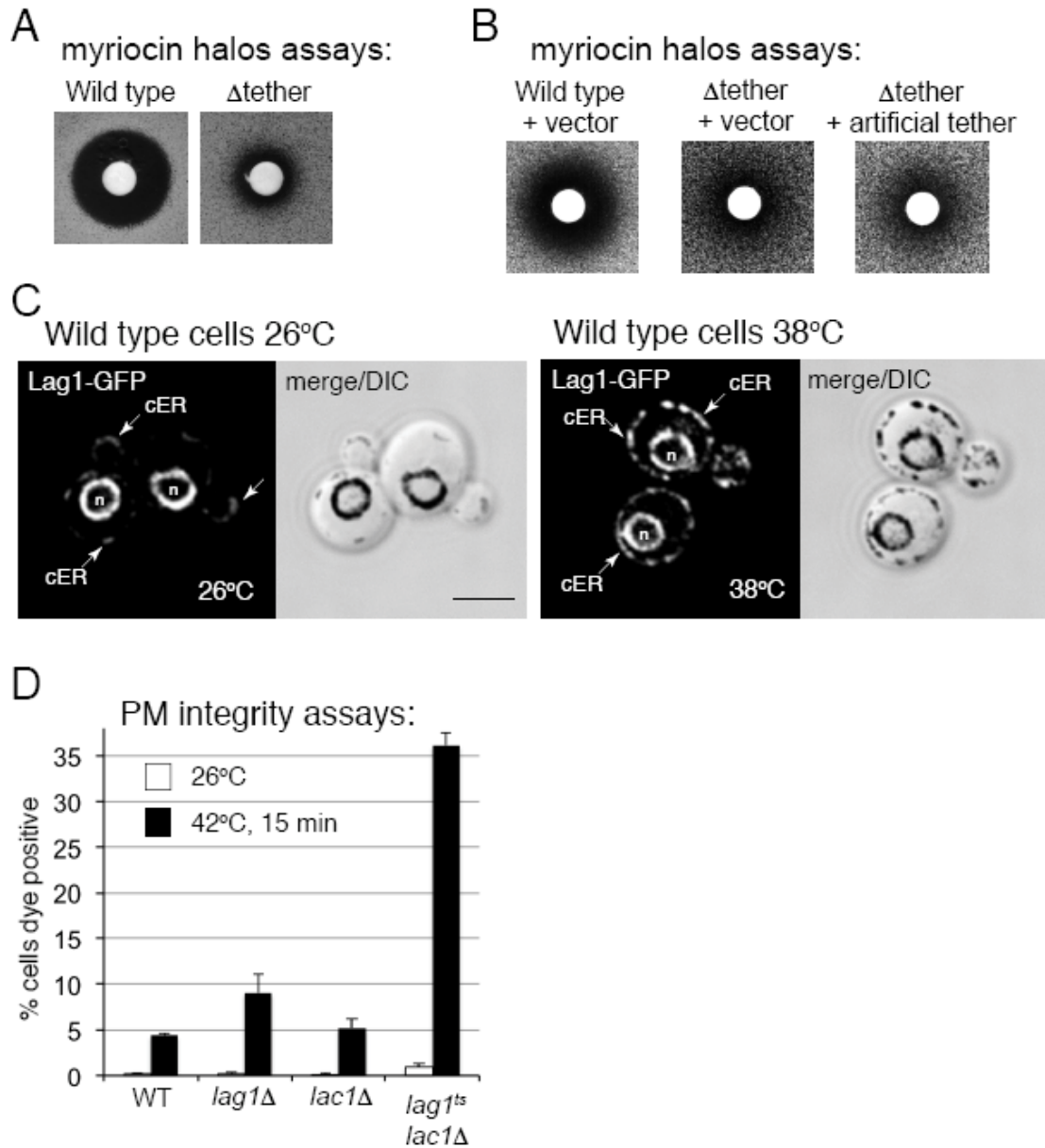cER
n
cER    38°C

D

PM integrity assays:



**Figure S6, related to Figure 6.ER-PM crosstalk controls ceramide synthase activity in the ER.**

A  TheΔtethercells are resistant to myriocin that inhibits LCB synthesis in the ER. Wild type or Δtether cells were plated as lawns on rich media and then overlaid with sterile filter discs containing 3 μl of a 1 mg/ml stock of myriocin in DMSO. After incubation at 26°C for 3 days, the plates were imaged. Wild type cells form a zone of growth inhibition (halos). The halos formed by Δtether cells are smaller in diameter indicating resistance to myriocin. See Figure 6A showing increased LCBs levels in the Δtether cells.

B Wild type cells carrying vector alone, Δtether cells carrying vector alone, and Δtether cells carrying a plasmid expressing the artificial tether protein 2xPH$^{PLC\delta}$-Scs2$^{129-244}$ (+A.T.) were plated as lawns on synthetic media and then overlaid with sterile filter discs containing 5μl of a 0.1 mg/ml stock of myriocin in DMSO. After incubation at 26°C for 3 days, the plates were imaged. Wild type cells form a zone of growth inhibition (halos). Expression of the artificial tether (+A.T.) did not rescue the myriocin resistance phenotype of the Δtethercells.

C Lag1-GFP localization in wildtype cells grown at 26°C (left panels). Lag1 localizes to nuclear ER surrounding the nucleus (n). Weak Lag1-GFP fluorescence in the cortical ER (cER) is indicated. Lag1-GFP localization in wildtype cells incubated at 38°C for 1 hour (right panels). Increased Lag1-GFP fluorescence in the cortical ER (cER) is observed. Scale bar, 3 μm.

D The Lag1 and Lac1 ceramide synthases have overlapping roles in maintaining PM integrity upon brief heat shock. Wildtype, *lag1Δ, lac1Δ,* and *lac1Δlag1$^{ts}$*cellswere incubated at 26°C (white bars) or 42°C for 10 minutes(black bars), stained with propidium iodide, and analyzed by flow cytometry.
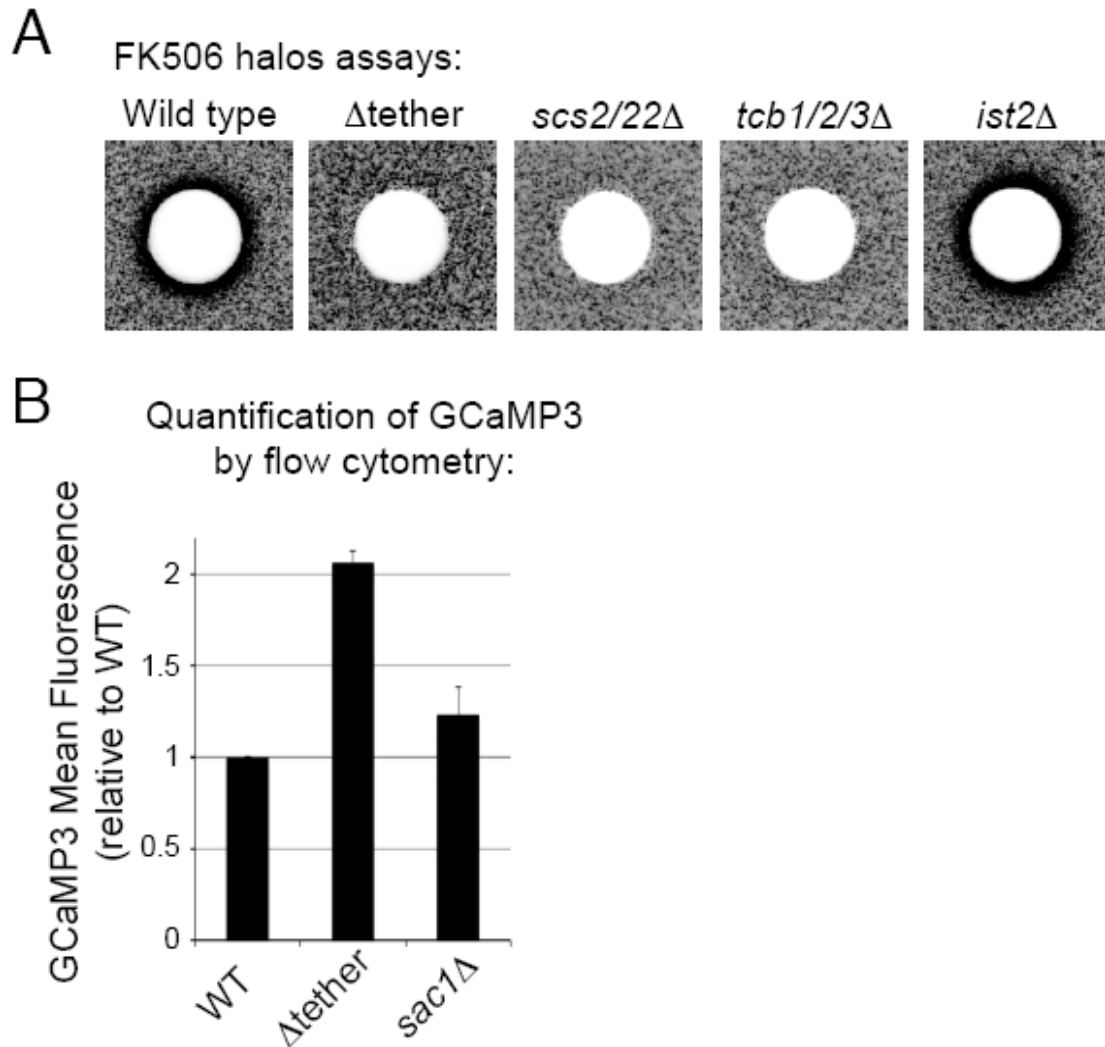
# Omnus *et al*., Figure S7

## A

FK506 halos assays:

| Wild type | Δtether | *scs2/22Δ* | *tcb1/2/3Δ* | *ist2Δ* |



## B

### Quantification of GCaMP3 by flow cytometry:



**Figure S7, related to Figure7.ER-PM junctions modulate cytoplasmic Ca$^{2+}$ and calcineurin phosphatase activity.**

AWildtype, Δtether, *scs2/22Δ*, *tcb1/2/3Δ*, and *ist2Δ* cells were plated as lawns and then overlaid with sterile filter discs containing 10μl of a 10 mg/ml stock of FK506in DMSO. After incubation at 26°C for 3 days, the plates were imaged. Wild type cells form a zone of growth inhibition (halos). The Δtether,*scs2/22Δ*, and *tcb1/2/3Δ*cells initially form halos (not shown), but recover and colonies form at FK506 concentrations inhibitory to the growth of wild type and *ist2Δ*cells.

BWild-type,Δtether, and *sac1Δ*cells expressing cytoplasmic GCaMP3 were grown at 26°C. The mean fluorescence intensity of GCaMP3 was quantified from cells (n=50,000) from each culture by flow cytometry. The data represent the means ± standard deviations from three independent experiments.

## Supplemental Tables

| | Table S1. Strains used in this study, related to the Materials and Methods. | |
|---|---|---|
| **Strain** | **Genotype** | **Reference/Source** |
| SEY6210 | *MATαleu2-3,112 ura3-52 his3Δ200 trp1-Δ901 lys2-801 suc2Δ9* | (Robinson *et al.*, 1988) |
| SEY6210.1 | *MAT**a**leu2-3,112 ura3-52 his3Δ200 trp1-Δ901 lys2-801 suc2Δ9* | (Robinson *et al.*, 1988) |
| AAY102 | SEY6210 *stt4Δ::HIS3* harboring pRS415*stt4-4* | (Audhya *et al.*, 2000) |
| AAY202 | SEY6210 *mss4Δ::HIS3* harboring YCp*lac*111*mss4$^{ts}$-102* | (Stefan *et al.*, 2002) |
| MFY55 | SEY6210 *sac1Δ::TRP1* | (Foti *et al.*, 2001) |
| MFY62 | SEY6210.1 *sac1Δ::TRP1* | (Foti *et al.*, 2001) |
| YCS226 | AAY102 except *sac1Δ::TRP1* | (Foti *et al.*, 2001) |
| YCS176 | SEY6210 *sjl1Δsjl2Δsjl3Δ* carrying pRS415*sjl2$^{ts}$-8* | (Stefan *et al.*, 2002) |
| ANDY198 | SEY6210.1 *ist2Δ::HISMX6scs2Δ::TRP1scs22Δ::HISMX6 tcb1Δ::KANMX6tcb2Δ::KANMX6 tcb3Δ::HISMX6* | (Manford *et al.*, 2012) |
| ANDY157 | SEY6210.1*SEC61-GFP::KANMX6* | (Manford *et al.*, 2012) |
| ANDY201 | ANDY198 *SEC61-GFP::KANMX6* | (Manford *et al.*, 2012) |
| MTY28 | SEY6210.1 *pkh1Δ::HIS3MX6pkh2Δ::HIS3MX6*harboring pRS415*pkh1$^{ts}$* | This study |
| MTY78 | SEY6210.1 *ypk1$^{ts}$::HIS3ypk2Δ::HIS3* | J. Thorner |
| MTY217 | SEY6210 *lac1Δ::HIS3MX6* | This study |
| MTY216 | SEY6210 *lag1Δ::HIS3MX6* | This study |
| MTY286 | SEY6210 *lag1Δ::HIS3MX6lac1Δ::HIS3MX6*harboring pRS414*lag1$^{ts}$* | This study |
| MTY287 | SEY6210.1 *lag1Δ::HIS3MX6lac1Δ::HIS3MX6*harboring pRS414*lag1$^{ts}$* | This study |
| MTY155 | SEY6210 *aur1Δ::HIS3MX6*harboring pRS414*aur1$^{ts}$* | (Tabuchi *et al.*, 2006) |
| YCS581 | SEY6210 *orm1Δ::HIS3MX6 orm2Δ::TRP1* | This study |
| RH144-3D | *MAT**a**lcb1-100 barl-1 his4 leu2 ura3* | H. Riezmann |
| YCS695 | SEY6210.1 *LAG1-GFP::NATMX6* | This study |
| YCS697 | ANDY198 *LAG1-GFP::NATMX6* | This study |
| YCS721 | MTY78 *LAG1-GFP::NATMX6* | This study |

**Table S2. Plasmids used in this study, related to the Materials and Methods.**

| Plasmid Name | Description | Source |
|---|---|---|
| pCS403 | pRS415-pGPD-mCherry-2xPH$^{Osh2}$ | This study |
| pYL95 | pRS415-pGPD-mCherry-2xPH$^{PLC\delta}$ | (Ling *et al.*, 2012) |
| pAM42 | pRS306-GFP-HDEL | (Manford *et al.*, 2012) |
| | pRS416-pGPD-mCherry-2xPH$^{PLC\delta}$□Scs2$^{129-244}$ | This study |
| pCS291 | pRS416-*CAN1*-GFP | (Lin *et al.*, 2008) |
| | pRS415-*stt4-4* | (Audhya *et al.*, 2000) |
| | YC*plac*111-*mss4$^{ts}$-102* | (Stefan *et al.*, 2002) |
| | pRS416-p*MET25*-*YPK1* | This study |
| | pRS416-GFP-*PKH1* | This study |
| | pRS416-*PKH1* | This study |
| | pRS416-*SLM1*-GFP | (Audhya *et al.*, 2004) |
| | pRS415-*LAG1* | This study |
| | pRS415-*LAG1$^{S23E\ S24E}$* | This study |
| pAMS366 | *CEN URA3* 4xCDRE-*lacZ* | (Stathopoulos and Cyert, 1997) |
| | pRS415-pGPD-GCaMP3 | This study |

**Table S3. GFP-Pkh1 localization upon modulation of cellular phosphoinositideand sphingolipid levels.**
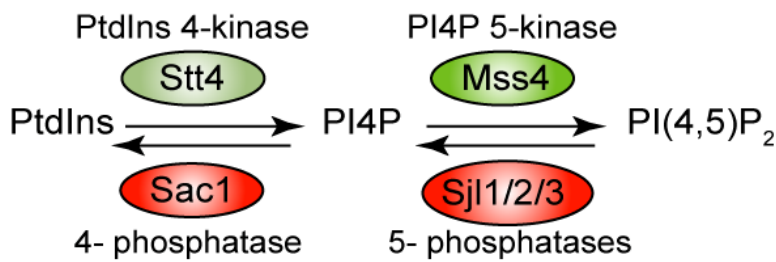


| Genotype + condition | Average GFP-Pkh1 puncta per mid-section | Number of cells |
|---|---|---|
| WT 26°C (DMSO) | 1.6 +/- 0.3 (STDEV) | 612 (n=3 experiments) |
| WT 42°C, 10 min (DMSO) | 4.3 +/- 1.3 (STDEV) | 837 (n=3 experiments) |
| WT 26°C (PAO) | 1.6 +/- 0.2 (STDEV) | 575 (n=3 experiments) |
| WT 42°C, 10 min (PAO) | 2.6 +/- 0.1 (STDEV) | 601 (n=3 experiments) |
| $stt4^{ts}$ 26°C | 2.1 | 190 (n=1 experiment) |
| $stt4^{ts}$ 42°C, 10 min | 3.9 | 109 (n=1 experiment) |
| $mss4^{ts}$ 26°C | 1.5 | 219 (n=1 experiment) |
| $mss4^{ts}$ 42°C, 10 min | 4.8 | 202 (n=1 experiment) |
| $sac1\Delta$ 26°C | 4 +/- 0.3 (STDEV) | 1802 (n=3 experiments) |
| $sjl1\Delta sjl2^{ts} sjl3\Delta$ 26°C | 4.8 +/- 0.2 (STDEV) | 469 (n=3 experiments) |
| $orm1\Delta orm2\Delta$ 26°C | 1.5 +/- 0.2 (STDEV) | 323 (n=3 experiments) |
| $orm1\Delta orm2\Delta$ 42°C, 10 min | 3 +/- 0.3 (STDEV) | 259 (n=3 experiments) |

GFP-Pkh1 maxima were identified and quantitated in single focal plane sections from cells grown at 26°C or following a brief heat shock for 10 minutes at 42°C using ImageJ. When indicated, cells were grown in media supplemented with PAO (final concentration 25μM) or an equal volume of DMSO for 2.5 hours prior toimage acquisition or heat shock at 42°C for 10 min followed by image acquisition.

## Supplemental Materials and Methods

### Yeast Strains, Plasmids, Media, and Growth Assays

Descriptions of strains and plasmids used in this study are in Supplemental Tables S1 and S2. Gene deletions and epitope tags were introduced into yeast by homologous recombination(Longtine *et al.*, 1998). Theshuttlevectors used in this study have been described previously(Sikorski and Hieter, 1989). Plasmids were sequenced to ensure that no mutations were introduced due to manipulations. Mutant constructs were generated by site directed mutagenesis (Quickchange, Stratagene) and confirmed by sequencing. Standard techniques and media were used for yeast and bacterialgrowth.For all plating assays, cells were grown to midlog, adjusted to 1 $OD_{600}$/ml, and serial dilutions were plated on the indicated media at the indicated temperatures.

### Fluorescence Microscopy

Fluorescence microscopy experiments were performed on mid-log yeast cultures in synthetic media at the appropriate temperatures. Imagesfor Figures 1A, S1D, S4D,S6C, and 7C were obtained using a DeltaVision RT microscopy system (Applied Precision) equipped with an IX71 Olympus microscope, a PlanApo 100X objective (1.35 NA, Olympus), DAPI, FITC, and rhodamine filters, and a Cool Snap HQ digital camera (Photometrics). Images were deconvolved using soft-WoRx 3.5.0 software (Applied Precision, LLC).  The brightness and contrast of images were linearly adjusted and cropped in Photoshop (Adobe). Results are

based on observations of >30cells in Figure S4D, 30 ROI from 10 cells in Figure 7C, and >100 cells for all other Figures and SupplementalFigures.

For Figures 1B and S1C, images of midlog cells were acquired with a CSU-X spinning disk microscope (Yokogawa) with a 63x1.4NA objective on an inverted microscope (DM16000B; Leica), a QuantEM EMCCD camera (Photometrics), and controlled by Slidebook 5.0 (Intelligent Imaging Innovations). The brightness and contrast of images were adjusted in Slidebook 5.0 and cropped in Photoshop (Adobe). Results are based on observations of >100 cells.

For Figures 4A-D,S4C, S4E, S4F, 5C, and Table S3, data was acquired with a PerkinElmer UltraviewVox spinning disk confocalmicroscope that consists of a Nikon TiE inverted stand attached to a Yokogawa CSU-X1 spinning disk scan head, a Hamamatsu C9100-13 EMCCD camera, Prior NanoscanZpiezo focus and a Nikon Perfect Focus System (PFS).Results are based on observations of >100 cells and in Figure 4>700 cells. The brightness and contrast of images were linearly adjusted and cropped in Photoshop (Adobe). Original, unadjusted data was used for high content quantitative cell imaging analyses (Figure 4 and Table S3).

**Quantitative Image Analysis**

Quantitative image analysis was conducted using ImageJ (Fiji). Specifically, points of interests (GFP-Pkh1 foci) were identified using the Find Maxima tool applying appropriate noise tolerance settings.

**Plasma Membrane Integrity Assays**

PM integrity assays were performed as described(Zhao *et al.*, 2013). Yeast strains were grown to midlog phase at $26^{o}$C and shifted to $40^{o}$C for 2 hr or $42^{o}$C for 10-15 min as indicated.1 $OD_{600}$ equivalent of cells was pelleted andresuspended in PBST (0.01% Tween 20), and cells were stained with propidium iodide (Sigma) for 15 min. Cells were then washed twice with $ddH_2O$ and analyzed by flow cytometryon a BD Accuri C6 flow cytometer.For flow cytometry analysis, 50,000 cells were counted for each sample from three independent experiments and combined for a total analysis of 150,000 cells. Background was determined by analyzing each of the cell strains at the indicated temperatures prior to staining with propidium iodide.

**Sphingolipid analysis.**

Metabolic labeling, lipid extraction, and TLC analysis of sphingolipids was performed as described (Tabuchi *et al.*, 2006). Before labeling, cells were grown in YNB medium with the appropriate amino acids. Midlog-phase cells were harvested and then shifted to the appropriate temperature for 10 min, followed by the addition of20 μCi of [$^3$H]serine (Perkin Elmer). After 60 min, cells were lysed in ice-cold 4.5% perchloric acid with glass beads to generate extracts. The extracts were subjected to centrifugation for 20 min at $4^{o}$C, and the pellets were washed once with ice-cold 100 mM EDTA. The perchloric acid-precipitable material was subjected to mild alkaline methanolysis for 50 min at 50°C. After mild alkaline methanolysis, the extracts were dried and samples were

resuspended in water by sonication to measure total incorporated [$^3$H]serine. The alkali-stable [$^3$H]serine-labeled lipids (sphingolipids) were extracted with water-saturated butanol twice and dried, and samples were resuspended in chloroform/methanol/water (10:10:3) and normalized by total incorporated [$^3$H]serine. Normalized samples were applied to Whatman Linear K6D silica gel thin-layer chromatography (TLC) plates and resolved in CHCl$_3$/methanol/4.2 N NH$_4$OH (9:7:2) for 75 min. This condition could discriminate the band of ceramide from the band of unknown lipid "X" (top band observed on TLC plates). Radioactive bands were visualized by X-ray film after treatment with En$^3$Hance (NEN Life Science Products). Relative levels of ceramides were determined using ImageJ and Adobe Photoshop software (measurement functions).Identification of each sphingolipid was done using treatment with known inhibitors of sphingolipid biosynthesis. We detected the band labelled "X," which appears at the top of each TLC plate, even under conditions where sphingolipid synthesis was completely blocked by treatment with myriocin, indicating that this lipid is likely not asphingolipid.

**Analysis of Cellular Protein Phosphorylation and Expression**

5 OD$_{600}$ equivalents of mid-log cells pretreated at the indicated temperatures were harvested by precipitation in 10% trichloroacidic acid (TCA). Precipitates were washed in acetone, aspirated, resuspended in lysis buffer (150 mMNaCl, 50mM Tris pH 7.5, 1mM EDTA, 1% SDS and a phosphatase inhibitor cocktail), and mechanically lysed with glass beads. Sample buffer (150 mMTris pH 6.8, 6M

Urea, 6%SDS, 10% β-mercaptoethanol, 20% Glycerol) was added and extracts were analyzed by SDS-PAGE. To detect phosphorylation-dependent mobility shifts of Lag1-GFP, whole-cell extracts were loaded onto 10% Phos-tag acrylamide gels (Wako Chemicals). Before transfer to nitrocellulose membranes, Phos-tag gels were washed twice for 10 min in transfer buffer containing 2 mM EDTA and then once for 10 min in transfer buffer without EDTA. Immunoblottingwas performed with the following antibodies: α-Pep12 (Invitrogen), α-G6PDH (Sigma), α-PGK (Novex), α-GFP (Santa Cruz Biotechnology or Roche), α-PKC (pan) zeta T410 (Cell Signaling) for phospho-Ypk1(T504), α-phospho-Ypk1(T662) (Niles *et al.*, 2012),α-Ypk1 (Cell Signaling), and α-phospho-p44/42 MAPK (Cell Signaling) for phospho-Slt2, and visualized using the appropriate secondary antibodies conjugated to HRP. Images were quantified using ImageQuant (GE Healthcare), ImageJ, and Adobe Photoshop software. For Figure E5B, secondary antibodies conjugated tofluorescent dyes (LI-COR Biosciences) were used and quantified on the Odyssey Infrared Imaging System (LI-COR Biosciences).

**β-Galactosidase Assays**

Strains harboring a *CDRE-lacZ* reporter plasmid(Stathopoulos and Cyert, 1997) were grown to midlog at 26$^{\circ}$C, and indicated samples were shifted to 38$^{\circ}$C for 2 hr. Harvested cells were washed 1x in Z buffer (60mM $Na_2HPO_4$, 40mM $NaH_2PO_4$ 10mM KCl, 1mM $MgSO_4$) and $OD_{600}$for each sample were measured. Samples were adjusted to 1000 · l in Z buffer, 50· l of 0.1% SDS was added,

and samples were vortexed for 15 seconds. 50·l of chloroform was then added

and samples were vortexed for 15 seconds. Reactions were started by the

addition of 100·l of ONPG (4mg/ml). 500·l of 1M $Na_2CO3$ was added to

quench the reaction and samples were cleared at 13000 x g for 2min. $Abs_{420}$ of

the supernatant was measured and the units of activity were calculated (1000 x

$Abs_{420}$)/(time (min) x $OD_{600}$ equivalents).

**Quantitative GCaMP3 Fluorescence Assays**

Strains expressing a cytoplasmic GCaMP3 reporter(Tian *et al.*, 2009) were

grown at $26^oC$.  For microscopic analysis, wildtype cells were labelled with CMAC

to stain vacuoles as previously described (Stefan and Blumer, 1999). The

cultures were mixed and observed on the same cover slip by fluorescence

microscopy as described above. Images were quantified using soft-WoRx 3.5.0

software (Applied Precision, LLC).For flow cytometry experiments, cells were

transferred to PBS. Mean fluorescence of 50,000 events was recorded on a BD

Accuri C6 flow cytometer. Background was determined using strains harbouring

vector alone. Results are the mean of three independent experiments performed

in triplicate. Error bars show standard deviation.

## Supplemental References

Audhya, A., and Emr, S.D. (2003). Regulation of PI4,5P2 synthesis by nuclear-cytoplasmic shuttling of the Mss4 lipid kinase. The EMBO journal *22*, 4223-4236.

Audhya, A., Foti, M., and Emr, S.D. (2000). Distinct roles for the yeast phosphatidylinositol 4-kinases, Stt4p and Pik1p, in secretion, cell growth, and organelle membrane dynamics. Molecular biology of the cell *11*, 2673-2689.

Audhya, A., Loewith, R., Parsons, A.B., Gao, L., Tabuchi, M., Zhou, H., Boone, C., Hall, M.N., and Emr, S.D. (2004). Genome-wide lethality screen identifies new PI4,5P2 effectors that regulate the actin cytoskeleton. The EMBO journal *23*, 3747-3757.

Foti, M., Audhya, A., and Emr, S.D. (2001). Sac1 lipid phosphatase and Stt4 phosphatidylinositol 4-kinase regulate a pool of phosphatidylinositol 4-phosphate that functions in the control of the actin cytoskeleton and vacuole morphology. Molecular biology of the cell *12*, 2396-2411.

Lin, C.H., MacGurn, J.A., Chu, T., Stefan, C.J., and Emr, S.D. (2008). Arrestin-related ubiquitin-ligase adaptors regulate endocytosis and protein turnover at the cell surface. Cell *135*, 714-725.

Ling, Y., Stefan, C.J., Macgurn, J.A., Audhya, A., and Emr, S.D. (2012). The dual PH domain protein Opy1 functions as a sensor and modulator of PtdIns(4,5)P(2) synthesis. The EMBO journal *31*, 2882-2894.

Longtine, M.S., McKenzie, A., 3rd, Demarini, D.J., Shah, N.G., Wach, A., Brachat, A., Philippsen, P., and Pringle, J.R. (1998). Additional modules for versatile and economical PCR-based gene deletion and modification in Saccharomyces cerevisiae. Yeast *14*, 953-961.

Manford, A.G., Stefan, C.J., Yuan, H.L., Macgurn, J.A., and Emr, S.D. (2012). ER-to-plasma membrane tethering proteins regulate cell signaling and ER morphology. Developmental cell *23*, 1129-1140.

Niles, B.J., Mogri, H., Hill, A., Vlahakis, A., and Powers, T. (2012). Plasma membrane recruitment and activation of the AGC kinase Ypk1 is mediated by target of rapamycin complex 2 (TORC2) and its effector proteins Slm1 and Slm2. Proceedings of the National Academy of Sciences of the United States of America *109*, 1536-1541.

Robinson, J.S., Klionsky, D.J., Banta, L.M., and Emr, S.D. (1988). Protein sorting in Saccharomyces cerevisiae: isolation of mutants defective in the delivery and

processing of multiple vacuolar hydrolases. Molecular and cellular biology *8*, 4936-4948.

Sikorski, R.S., and Hieter, P. (1989). A system of shuttle vectors and yeast host strains designed for efficient manipulation of DNA in Saccharomyces cerevisiae. Genetics *122*, 19-27.

Stathopoulos, A.M., and Cyert, M.S. (1997). Calcineurin acts through the CRZ1/TCN1-encoded transcription factor to regulate gene expression in yeast. Genes & development *11*, 3432-3444.

Stefan, C.J., Audhya, A., and Emr, S.D. (2002). The yeast synaptojanin-like proteins control the cellular distribution of phosphatidylinositol (4,5)-bisphosphate. Molecular biology of the cell *13*, 542-557.

Stefan, C.J., and Blumer, K.J. (1999). A syntaxin homolog encoded by VAM3 mediates down-regulation of a yeast G protein-coupled receptor. The Journal of biological chemistry *274*, 1835-1841.

Stradalova, V., Blazikova, M., Grossmann, G., Opekarova, M., Tanner, W., and Malinsky, J. (2012). Distribution of cortical endoplasmic reticulum determines positioning of endocytic events in yeast plasma membrane. PloS one *7*, e35132.

Tabuchi, M., Audhya, A., Parsons, A.B., Boone, C., and Emr, S.D. (2006). The phosphatidylinositol 4,5-biphosphate and TORC2 binding proteins Slm1 and Slm2 function in sphingolipid regulation. Molecular and cellular biology *26*, 5861-5875.

Tian, L., Hires, S.A., Mao, T., Huber, D., Chiappe, M.E., Chalasani, S.H., Petreanu, L., Akerboom, J., McKinney, S.A., Schreiter, E.R., Bargmann, C.I., Jayaraman, V., Svoboda, K., and Looger, L.L. (2009). Imaging neural activity in worms, flies and mice with improved GCaMP calcium indicators. Nature methods *6*, 875-881.

Zhao, Y., Macgurn, J.A., Liu, M., and Emr, S. (2013). The ART-Rsp5 ubiquitin ligase network comprises a plasma membrane quality control system that protects yeast cells from proteotoxic stress. eLife *2*, e00459.